Supporting Information

A Novel [Os(1,10-phenanthroline-5,6-dione)$_2$(PVP)$_4$Cl]Cl Redox Polymer for Electrocatalytic Oxidation of NADH and its Application to the Construction of Reagentless β–D-glucose Biosensors

Valeri Pavlov[1], Óscar Rincón[2], Sonia Solé[1], Arantzazu Narváez[2], Elena Domínguez[2], Ioanis Katakis[1]*

[1]Bioanalysis and Bioelectrochemistry Group, Chemical Engineering, Universitat Rovira i Virgili, E-43006, Tarragona (Catalonia), Spain. [2]Departamento de Química Analítica, Universidad de Alcalá, E-28871 Alcalá de Henares (Madrid), Spain.

EXPERIMENTAL SECTION

Materials. β–Dihydronicotinamide adenine dinucleotide (NADH), β–nicotinamide adenine dinucleotide (NAD^+), were purchased from Sigma (Madrid, Spain). Glucose dehydrogenase (GDH) (EC 1.1.1.47) from *Bacillus megaterium* (220 U/mg protein) was obtained from Merck (Darmstadt, Germany). Sodium phosphate salts, sodium chloride and dimethylformamide were from Aldrich (Madrid, Spain). Ethylene glycol and β–D-glucose were purchased from Panreac (Madrid, Spain). Poly(ethylene glycol) diglycidyl ether (PEGDGE) and poly(4-vinyl pyridine) (PVP) were obtained from Polysciences Inc. (Warrington, PA, USA). Spectrographic graphite rods were acquired from Carbone of America Corp. Ultra Carbon Division (Bay City, MI, USA). Fine emery paper was from Buehler Ltd. (Lake Bluff, IL, USA). All other reagents were of analytical grade. Water was produced in a Mili-Q^{TM} system (Millipore Corp., Bedford, MA, USA). [Os(1,10-phenanthroline-5,6-dione)$_2$Cl$_2$] was synthesized according to an earlier published modified method.[28,31] The ^{1}H NMR investigation performed in $(CD_3)_2SO$ with a tetramethylsilane standard demonstrated following shifts δ_H: 8.1 ppm (2H dd), 7.53 ppm (2H dd), and 7.15 ppm (2H dd). Poly(4-vinyl pyridine) was derivatized with bromoethylamine as reported elsewhere[62] to yield the "binder" polymer.

Synthesis of Os-phendione-PVP. 80 mg of [Os(1,10-phenanthroline-5,6-dione)$_2$Cl$_2$] and 50 mg of poly(4-vinylpyridine) were mixed in 3 mL ethylene glycol. The mixture was deaerated with argon during 10 min and refluxed under argon in darkness during 1 h, the temperature of the oil bath being maintained below 220^{o}C, next the reaction mixture was cooled to room temperature and added dropwise to

100 mL of aqueous 1 M sodium chloride solution during 15 min. The resulting mixture was left to stay overnight at 4°C, the precipitate was filtered off, washed with water and air-dried. The synthesis route and the suggested structure of the resulting redox polymer is shown in Figure1. [Anal. Calcd. For n=4: C, 61.52%; H, 1.76%; N, 10.99%. Found: C, 61.71%; H, 1.70%; N, 10.7%.

Preparation of electrodes modified with Os-phendione-PVP. Spectrographic graphite rods of 3 mm diameter were fixed inside heat shrunk PVC tubes. Before use they were wet polished on fine (grit 400 and 600) emery paper to produce graphite electrodes having a flat circular surface.

Modification of the surface of electrodes was carried out by spreading of 1 μL on an electrode of 1.8 mg/mL Os-phendione-PVP solution in ethylene glycol. The polymer solution was left on the electrode surface for 3 min, the surface was washed with 2-3 drops of ethylene glycol and deionised water. The surface coverage was determined at pH 5.0 from the areas under the peak of cyclic voltammograms of phendione ligands at 10 mV s^{-1} assuming that four electrons were exchanged.

Preparation of *β*–D-glucose biosensors. A mixture containing 8.5 mg/mL "binder" polymer, 34 mg/mL NAD^+, 1 mg/mL PEGDGE, and 28 U/mL glucose dehydrogenase in 0.04 M sodium phosphate buffer (pH 7.6) was composed. Next 5 μL of the resulting mixture were placed on an Os-phendione-PVP modified electrode and dried under vacuum during 12 h.

Electrochemical measurements. For both amperometry and cyclic voltammetry a three-electrode conventional thermostabilised cell (3 mL) equipped with a $Ag/AgCl/KCl_{sat}$ reference electrode, and a platinum auxiliary electrode was used, a graphite electrode, modified according to one of the above mentioned procedures, being the working electrode. The buffer, pH 6.0 (0.1 M sodium phosphate and 0.15 M sodium chloride) served as supporting electrolyte. The pH was adjusted using concentrated NaOH or H_3PO_4. A computer-controlled BAS CV-50W voltammetric analyser (Bioanalytical Systems Inc., West Lafayette, IN, USA) was employed in cyclic voltammetry and steady state rotating electrode measurements. The rotating disk electrode, having the same spectrographic graphite as disk material, was operated by a modulated speed rotator AMSFRX (Pine Instruments Co., Grove City, PA, USA). The response to successive additions of stock β-*D*-glucose was registered as the steady state current with a computer controlled three-electrode potentiostat AUTOLAB PGSTAT 10 (Eco Chemie BV, The Netherlands). The working potential was 150 mV *vs.* $Ag/AgCl/KCl_{sat}$ and the temperature of the thoroughly stirred solution was 25°C unless indicated otherwise.

Electrochemical Conversion Experiments. Electrodes were prepared by fixing spectrographic graphite rods having diameter of 6 mm inside a heat shrunk PVC. They were wet polished on fine (grit 400 and 600) emery paper, cleaned by sonication, air-dried and modified with 4 μL of 1.8 mg/mL Os-phendione-PVP solution according to the above mentioned procedure. Next they were immersed into 2 mL of 18 μM NADH solution in 0.1 M phosphate buffer (pH 6.0) deaerated with argon, and poised at 150 mV *vs.* $Ag/AgCl/KCl_{sat}$ with stirring in a three-electrode electrochemical cell at 25 ºC. Spectrophotometrical measurements of absorbance at 340 nm (A_{340}) were used to determine the depletion of the NADH concentration during 1 hour (A_{340} changed from 0.1117 in the beginning to 0.0540 at the end of experiment, RSD 5%). Then, 1 mL of the resulting solution was mixed with 30 μL of a mixture

containing glucose dehydrogenase and 50 fold excess of glucose and the recovery of NADH concentration was monitored spectrophotometrically until reaching the end point (A_{340} equal to 0.0867). These values were corrected for the ΔA_{340} (from 0.1117 to 0.0902, RSD 6%) of a controlled solution of NADH during 1 hour which was not subjected to electrolysis in order to quantify the spontaneous decomposition of NADH. The area under the chronoamperometric plots was assessed to find the charge passed through the circuit during the electrocatalytic NADH oxidation which was equal to (2.3±0.3) mC.

STEADY-STATE KINETIC MODEL OF BIOSENSORS

Figure 8S illustrates the kinetic scheme for the operation of reagentless biosensors based on a dehydrogenase enzyme (E) catalyzing the reaction of NAD^+ (A) with a substrate (B) to give NADH (P) and a product (Q). Then a mediator (M), which has reduced (M_{red}) and oxidized (M_{ox}) forms, immobilized on the electrode surface, catalyzes the electrochemical conversion of P back to A. A_{im} and P_{im} are the concentrations of immobilized A and P. B_o and Q_o are the concentrations of the substrate and the product inside of the hydrogel. B_∞ and Q_∞ are the concentrations of the substrate and the product in the external medium. k'_B and k'_Q are mass transfer constants of the substrate and the product (cm s^{-1}), respectively. L is the thickness of the hydrogel layer. The following expressions for the flux of P to the electrode surface (j_{el}), which determines the current density of a biosensor (j) through the expression $j = nFj_{el}$, where n is the number of exchanged electrons and F is the Faraday's constant, can be obtained:

$$j_{el} = k'_B(B_\infty - B_o) \quad (1S)$$
$$j_{el} = L(k_3 A_{im}[E] - k_{-3}[E\cdot A]) \quad (2S)$$
$$j_{el} = L(k_4 B_o[E\cdot A] - k_{-4}[E\cdot A\cdot B]) \quad (3S)$$
$$j_{el} = L(k_5 [E\cdot A\cdot B] - k_{-5}[E\cdot P\cdot Q]) \quad (4S)$$
$$j_{el} = L(k_6 [E\cdot P\cdot Q] - k_{-6}[E\cdot P]Q_o) \quad (5S)$$
$$j_{el} = L(k_7 [E\cdot P] - k_{-7}[E]P_{im}) \quad (6S)$$
$$j_{el} = k'_Q Q_o \quad (7S)$$
$$j_{el} = k_1 P_{im}\Gamma_{Mox} - k_{-1}\Gamma_{M\cdot P} \quad (8S)$$
$$j_{el} = k_2 \Gamma_{M\cdot P} \quad (9S)$$
$$j_{el} = k_S\Gamma_{Mred} \quad (10S)$$
$$E_t = [E] + [E\cdot A] + [E\cdot A\cdot B] + [E\cdot P\cdot Q] + [E\cdot P] \quad (11S)$$
$$\Gamma = \Gamma_{M\cdot P} + \Gamma_{Mox} + \Gamma_{Mred} \quad (12S)$$
$$A_t = A_{im} + P_{im} \quad (13S)$$

Where Γ_{Mox} and Γ_{Mred} are surface coverages of the mediator in oxidized and reduced forms, respectively. Γ is the total mediator surface coverage. $\Gamma_{M\cdot P}$ is the surface coverage of the intermediate complex between the mediator and NADH. A_t and E_t are the total concentrations of the cofactor and the enzyme immobilized in the hydrogel, respectively. A_{im} and P_{im} are the concentrations of NAD^+ and NADH in the hydrogel respectively. The equations(2S-6S, 11S) yield the equation (14S) describing the enzyme kinetics.

$$j_{el} = \frac{E_t L(k_3k_4k_5k_6k_7A_{im}B_o - k_{-3}k_{-4}k_{-5}k_{-6}k_{-7}P_{im}Q_o)}{K_6k_7k_{-3}k_{-4} + k_{-3}k_5k_6k_7 + k_7k_{-3}k_{-4}k_{-5} + (k_3k_6k_7k_{-4} + k_3k_5k_6k_7 + k_3k_7k_{-4}k_{-5})A_{im} + k_4k_5k_6k_7B_o + (k_3k_4k_6k_7 + k_3k_4k_7k_{-5} + k_3k_4k_5k_7 + k_3k_4k_5k_6)A_{im}B_o + (k_6k_{-3}k_{-4}k_{-7} + k_5k_6k_{-3}k_{-7} + k_{-3}k_{-4}k_{-5}k_{-7})P_{im} + k_{-3}k_{-4}k_{-5}k_{-6}Q_o + (k_{-4}k_{-5}k_{-6}k_{-7} + k_{-3}k_{-5}k_{-6}k_{-7} + k_{-3}k_{-4}k_{-6}k_{-7} + k_5k_{-3}k_{-6}k_{-7})P_{im}Q_o + k_3k_{-4}k_{-5}k_{-6}A_{im}Q_o + (k_4k_{-5}k_{-6}k_{-7} + k_4k_5k_{-6}k_{-7})B_oP_{im}Q_o + (k_3k_4k_{-5}k_{-6} + k_3k_4k_5k_{-6})A_{im}B_oQ_o + k_4k_5k_6k_{-7}B_oP_{im}} \quad (14S)$$

When numerator and denominator of this rate equation are multiplied by the factor $(k_{-3}k_{-4}k_{-5}k_{-6}k_{-7})/((k_3k_4k_6k_7 + k_3k_4k_7k_{-5} + k_3k_4k_5k_7 + k_3k_4k_5k_6)(k_{-4}k_{-5}k_{-6}k_{-7} + k_{-3}k_{-5}k_{-6}k_{-7} + k_{-3}k_{-4}k_{-6}k_{-7} + k_5k_{-3}k_{-6}k_{-7}))$ the following equation can be obtained:

$$j_{el} = \frac{L(V_1V_2A_{im}B_o - (V_1V_2P_{im}Q_o)/K_{eq})}{K_{AB}V_2 + K_BV_2A_{im} + K_AV_2B_o + V_2A_{im}B_o + K_QV_1P_{im}/K_{eq} + K_PV_1Q_o/K_{eq} + V_1P_{im}Q_o/K_{eq} + K_PV_1A_{im}Q_o/(K_{iA}K_{eq}) + K_AV_2B_oP_{im}Q_o/(K_{iP}K_{iQ}) + K_PV_1A_{im}B_oQ_o/(K_{iA}K_{iB}K_{eq}) + K_AV_2B_oP_{im}/K_{iP}} \quad (15S)$$

Where $V_1 = E_t(k_4k_5k_6k_7)/(k_4k_6k_7 + k_4k_7k_{-5} + k_4k_5k_7 + k_4k_5k_6)$ and $V_2 = E_t(k_{-3}k_{-4}k_{-5}k_{-6})/(k_{-4}k_{-5}k_{-6} + k_{-3}k_{-5}k_{-6} + k_{-3}k_{-4}k_{-6} + k_5k_{-3}k_{-6})$ are the maximum velocities in forward and reverse directions, the equilibrium constant $K_{eq} = (k_3k_4k_5k_6k_7)/(k_{-3}k_{-4}k_{-5}k_{-6}k_{-7})$, Michaelis constants for A, B, P, Q are $K_A = (k_5k_6k_7)/(k_3k_6k_7 + k_3k_7k_{-5} + k_3k_5k_7 + k_3k_5k_6)$, $K_B = (k_6k_7k_{-4} + k_5k_6k_7 + k_7k_{-4}k_{-5})/(k_4k_6k_7 + k_4k_7k_{-5} + k_4k_5k_7 + k_4k_5k_6)$, $K_P = (k_{-3}k_{-4}k_{-5})/(k_{-4}k_{-5}k_{-7} + k_{-3}k_{-5}k_{-7} + k_{-3}k_{-4}k_{-7} + k_5k_{-3}k_{-7})$, $K_Q = (k_6k_{-3}k_{-4} + k_5k_6k_{-3} + k_{-3}k_{-4}k_{-5})/(k_{-4}k_{-5}k_{-6} + k_{-3}k_{-5}k_{-6} + k_{-3}k_{-4}k_{-6} + k_5k_{-3}k_{-6})$, the inhibition constants for A, B, P, Q are $K_{iA} = k_{-3}/k_3$, $K_{iB} = (k_{-4}k_{-5}k_{-6} + k_{-3}k_{-5}k_{-6} + k_{-3}k_{-4}k_{-6} + k_5k_{-3}k_{-6})/(k_4k_{-5}k_{-6} + k_4k_5k_{-6})$, $K_{iP} = k_7/k_{-7}$, $K_{iQ} = (k_5k_6)/(k_{-5}k_{-6} + k_5k_{-6})$ and $K_{AB} = (k_6k_7k_{-3}k_{-4} + k_{-3}k_5k_6k_7 + k_7k_{-3}k_{-4}k_{-5})/(k_3k_4k_6k_7 + k_3k_4k_7k_{-5} + k_3k_4k_5k_7 + k_3k_4k_5k_6) = K_BK_{iA}$, $K_{PQ} = (k_6k_7k_{-3}k_{-4} + k_{-3}k_5k_6k_7 + k_7k_{-3}k_{-4}k_{-5})/(k_{-4}k_{-5}k_{-6}k_{-7} + k_{-3}k_{-5}k_{-6}k_{-7} + k_{-3}k_{-4}k_{-6}k_{-7} + k_5k_{-3}k_{-6}k_{-7}) = K_QK_{iP}$

Dividing numerator and denominator of (15S) by V_2 and taking into account that $V_1/(V_2K_{eq}) = (K_BK_{iA})/(K_QK_{iP})$ one can derive the equation (16S):

$$j_{el} = \frac{L(V_1A_{im}B_o - (V_1P_{im}Q_o)/K_{eq})}{K_{AB} + K_BA_{im} + K_AB_o + A_{im}B_o + K_BK_{iA}P_{im}/K_{iP} + K_PK_BK_{iA}Q_o/(K_QK_{iP}) + K_BK_{iA}P_{im}Q_o/(K_QK_{iP}) + K_PK_BK_{iA}A_{im}Q_o/(K_QK_{iA}K_{iP}) + K_AB_oP_{im}Q_o/(K_{iP}K_{iQ}) + K_BK_PA_{im}B_oQ_o/(K_QK_{iB}K_{iP}) + K_AB_oP_{im}/K_{iP}} \quad (16S)$$

The equations (8S-10S, 12S) give the equation (17S) which governs the kinetics of NADH oxidation at the electrode surface modified with the mediator

$$j_{el} = \frac{\Gamma k_1 k_2 k_S P_{im}}{k_2 k_S + k_{-1} k_S + (k_1 k_2 + k_1 k_S) P_{im}} = \frac{\Gamma P_{im} k_1 k_2 k_S / (k_1 k_2 + k_1 k_S)}{(k_2 k_S + k_{-1} k_S)/(k_1 k_2 + k_1 k_S) + P_{im}} = \frac{k_{cat} \Gamma P_{im}}{K_M + P_{im}} \quad (17S)$$

where the Michaelis constant for the mediator M is $K_M = (k_2 k_S + k_{-1} k_S)/(k_1 k_2 + k_1 k_S)$ and $k_{cat} = k_2 k_S/(k_2 + k_S)$. Using the equations (13S) and (17S) the concentrations of NAD^+ and NADH (A_{im} and P_{im}) as well as B_o and Q_o from (1S) and (7S) can be found: $P_{im} = j_{el} K_M/(k_{cat}\Gamma - j_{el})$, $A_{im} = A_t - P_{im} = A_t - j_{el} K_M/(k_{cat}\Gamma - j_{el})$, $B_o = B_\infty - j_{el}/k'_B$, $Q_o = j_{el}/k'_Q$. Substitution of A_{im}, B_o, P_{im}, Q_o in equation (16S) by their expressions gives following equation:

$$\begin{aligned} j_{el} = {} & \frac{L(V_1(A_t - j_{el}K_M/(k_{cat}\Gamma - j_{el}))(B_\infty - j_{el}/k'_B) - (V_1(j_{el}K_M/(k_{cat}\Gamma - j_{el}))(j_{el}/k'_Q))/K_{eq})}{K_{AB} + K_B(A_t - j_{el}K_M/(k_{cat}\Gamma - j_{el})) + K_A(B_\infty - j_{el}/k'_B) + (A_t - j_{el}K_M/(k_{cat}\Gamma - j_{el}))(B_\infty - j_{el}/k'_B) + \\ & K_B K_{iA}(j_{el}K_M/(k_{cat}\Gamma - j_{el}))/K_{iP} + K_P K_B K_{iA}(j_{el}/k'_Q)/(K_Q K_{iP}) + K_B K_{iA}(j_{el}K_M/(k_{cat}\Gamma - j_{el}))(j_{el}/k'_Q)/(K_Q K_{iP}) + \\ & K_P K_B K_{iA}(A_t - j_{el}K_M/(k_{cat}\Gamma - j_{el}))(j_{el}/k'_Q)/(K_Q K_{iA} K_{iP}) + K_A(B_\infty - j_{el}/k'_B)(j_{el}K_M/(k_{cat}\Gamma - j_{el}))(j_{el}/k'_Q)/(K_{iP} K_{iQ}) + \\ & K_B K_P(A_t - j_{el}K_M/(k_{cat}\Gamma - j_{el}))(B_\infty - j_{el}/k'_B)(j_{el}/k'_Q)/(K_Q K_{iB} K_{iP}) + K_A(B_\infty - j_{el}/k'_B)(j_{el}K_M/(k_{cat}\Gamma - j_{el}))/K_{iP} \end{aligned} \quad (18S)$$

The latter is transformed into the equation of the fourth order:

$$\begin{aligned} & LV_1\Gamma k_{cat}A_t B_\infty = j_{el}[K_{AB}\Gamma k_{cat} + K_A\Gamma k_{cat}B_\infty + \Gamma k_{cat}A_t B_\infty + K_B\Gamma k_{cat}A_t + LV_1((A_t + K_M)k'_B B_\infty + \\ & \Gamma k_{cat}A_t)/k'_B] + j^2_{el}[V_1 LK_M/(K_{eq}k'_Q) + K_B K_{iA}K_M/K_{iP} + K_P K_B K_{iA}\Gamma k_{cat}/(K_Q K_{iP}k'_Q) + \\ & K_P K_B K_{iA}\Gamma k_{cat}A_t/(K_Q K_{iA} K_{iP}k'_Q) + \Gamma k_{cat}A_t B_\infty k'_B K_B K_P/(K_Q K_{iB} K_{iP}k'_B k'_Q) + K_M K_A B_\infty/K_{iP} - LV_1(A_t + K_M)/k'_B - \\ & K_{AB} - K_B(A_t + K_M) - (k'_B B_\infty + \Gamma k_{cat})K_A/k'_B - (A_t + K_M)B_\infty - \Gamma k_{cat}A_t/k'_B] + j^3_{el}[K_A/k'_B + (A_t + K_M)/k'_B + \\ & K_M K_B K_{iA}/(K_Q K_{iP}k'_Q) + K_M K_A B_\infty/(K_{iP}K_{iQ}k'_Q) - K_P K_B K_{iA}/(K_Q K_{iP}k'_Q) - (A_t + K_M)K_P K_B K_{iA}/(K_Q K_{iA} K_{iP}k'_Q) - \\ & K_M K_A/(K_{iP}k'_B) - (\Gamma k_{cat}A_t)K_B K_P/(K_Q K_{iB} K_{iP}k'_B k'_Q) - (A_t + K_M)B_\infty K_B K_P/(K_Q K_{iB} K_{iP}k'_Q)] + \\ & j^4_{el}[(A_t + K_M)K_B K_P/(K_Q K_{iB} K_{iP}k'_B k'_Q) - K_M K_A/(K_{iP}K_{iQ}k'_B k'_Q)] \end{aligned} \quad (19S)$$

In some enzymatic reactions, including the reaction catalyzed by GDH, the equilibrium is greatly shifted towards the formation of the reaction products and their concentrations P_o and Q_o exert negligible influence on the reaction rate. In this case the equation (16S) can be rewritten as follows:

$$j_{el} = \frac{LV_1 A_{im} B}{K_{AB} + K_B A_{im} + K_A B_o + A_{im} B_o} = \frac{LV_1(A_t - j_{el}K_M/(k_{cat}\Gamma - j_{el}))(B_\infty - j_{el}/k'_B)}{K_{AB} + K_B(A_t - j_{el}K_M/(k_{cat}\Gamma - j_{el})) + K_A(B_\infty - j_{el}/k'_B) + (A_t - j_{el}K_M/(k_{cat}\Gamma - j_{el}))(B_\infty - j_{el}/k'_B)} \quad (20S)$$

or

$$\begin{aligned} & LV_1\Gamma k_{cat}k'_B A_t B_\infty = j_{el}[K_{AB}k'_B\Gamma k_{cat} + K_B k'_B\Gamma k_{cat}A_t + K_A k'_B\Gamma k_{cat}B_\infty + \Gamma k_{cat}k'_B A_t B_\infty + LV_1\Gamma k_{cat}A_t + \\ & LV_1 k'_B(A_t + K_M)B_\infty] - j^2_{el}[K_{AB}k'_B + K_B k'_B(A_t + K_M) + K_A k'_B B_\infty + K_A\Gamma k_{cat} + \Gamma k_{cat}A_t + k'_B(A_t + K_M)B_\infty + \\ & LV_1(A_t + K_M)] + j^3_{el}[K_A + A_t + K_M] \end{aligned} \quad (21S)$$

If the concentration of the immobilized cofactor A_t is so high that it is not a limiting factor of the enzymatic reaction the equation 21S can be simplified to give:

$$LV_1\Gamma k_{cat}k'_B B_\infty = j_{el}[K_B k'_B \Gamma k_{cat} + \Gamma k_{cat}k'_B B_\infty + LV_1\Gamma k_{cat} + LV_1 k'_B B_\infty] - j^2_{el}[K_B k'_B + \Gamma k_{cat} + k'_B B_\infty + LV_1] + j^3_{el} \quad (22S)$$

When the concentration of the substrate B_∞ is infinitely high the latter equation can be rewritten as:

$$LV_1\Gamma_M k_{cat}k'_B = j_{el\,max}[\Gamma_M k_{cat}k'_B + LV_1 k'_B] - j^2_{el\,max}k'_B \quad (23S)$$

$$j^2_{el\,max} - j_{el\,max}[\Gamma_M k_{cat} + LV_1] + LV_1\Gamma_M k_{cat} = 0 \quad (24S)$$

The roots of this square equation are $j_{el\,max\,1} = \Gamma k_{cat}$ (25S)

and

$$j_{el\,max\,2} = LV_1 \quad (26S)$$

It follows from the equation (24S) that the maximum flux in reagentless biosensors in the presence of saturating concentration of NAD^+ is equal to LV_1 (the maximum response is limited by the enzymatic reaction) or Γk_{cat} (the maximum response is limited by the reaction of the mediated oxidation of NADH at the electrode surface). The value of the maximum flux of the electrochemical NADH oxidation (Γk_{cat}) was found from calibration curves of the graphite electrodes modified with Os-phendione-PVP according to the Eadie-Hofstee plots. Calibration of these electrodes with NADH was performed to demonstrate the maximum current density of 492 μA cm^{-2} which corresponds to Γk_{cat} equal to 2.55x10^{-9} mol s^{-1} cm^{-2}.

Cubic equation (21S), having exact analytical solution, was used to simulate the response of reagentless glucose biosensors. The typical calibration curves and the Eadie-Hofstee plots for glucose biosensors computed at varied loading of NAD^+ (A_t), the infinitively rapid mass transport of glucose ($k'_B \rightarrow \infty$), and the maximum flux of the enzymatic reduction of NAD^+ (LV_1) less than the maximum flux of the electrochemical oxidation of NADH (Γk_{cat}) are represented in the Figure 9S. The straight lines of the Eadie-Hofstee plots indicate that under these conditions the response of the biosensors is determined only by the rate of the enzymatic reduction of NAD^+. The slope of the Eadie-Hofstee plots which is equal to $-1/K_{B\ app}$, where $K_{B\ app}$ is the apparent Michaelis constant for the substrate B, depends on the loading of NAD^+. The intercept of the Eadie-Hofstee plots with the axis of j which is the apparent maximum current density ($j_{max\ app}$) is determined by A_t too. So, an increase in the loading of NAD^+ results in a rise in the apparent Michaelis constant and the maximum current density. Only when the NAD^+ loading reaches a saturating level ($A_t \rightarrow \infty$) the values of the apparent maximum current density ($j_{max\ app}$) and the apparent Michaelis constant ($K_{B\ app}$) coincide with those of the product LV_1nF and the Michaelis constant (K_B) respectively.

The Figure 10S demonstrates the effect of the mass transfer constant of the substrate (k'_B) on the calibration curves and the Eadie-Hofstee plots simulated with the saturating loading of NAD^+ ($A_t \rightarrow \infty$) and the maximum flux of the enzymatic reduction of NAD^+ (LV_1) less than the maximum flux of the electrochemical oxidation of NADH (Γk_{cat}). In this case the smaller is the mass transfer constant of the

substrate the greater is the deviation from the straight line in the Eadie-Hofstee plots which is characteristic of the process governed by the enzymatic reaction of the NAD^+ reduction. The values of the apparent current densities and apparent Michaelis constants obtained by the Eadie-Hofstee plots coincide with the values of LV_1nF. and K_B, respectively, only if very high concentrations of the substrate (B_∞) are used to build the plots

The Figures 11S-18S show the influence of the maximum flux of the electrochemical NADH oxidation (Γk_{cat}), maximum flux of the enzymatic reduction of NAD^+ (LV_1), and the NAD^+ loading on calibration curves and the Eadie-Hofstee plots simulated with the infinitively rapid mass transport of glucose ($k'_B \rightarrow \infty$). Clearly, the maximum current density is determined by the maximum flux of the enzymatic reduction of NAD^+ (LV_1) when the latter is less than the maximum flux of the electrochemical NADH oxidation (Γk_{cat}). The maximum flux of the electrochemical NADH oxidation (Γk_{cat}) limits the maximum current density if Γk_{cat} is less than the flux of the enzymatic reduction of NAD^+ at given NAD^+ loading (A_t). The sharp breaks followed by the horizontal lines in the Figures 11S, 12S, 15S, 16S are due to NAD^+ depletion caused by rapid enzymatic reaction at the saturating NAD^+ loading in the steady state model. The decrease in the NAD^+ loading results in the decrease in the flux of the enzymatic reduction of NAD^+ (Figures 13S, 17S) making that less or equal to the flux of the electrochemical NADH oxidation at a given value of A_t. That's why, at low NAD^+ loading the response of the biosensors is limited by the enzymatic reduction of NAD^+ even if Γk_{cat} is less than LV_1 (Figures 14S, 18S). The Eadie-Hofstee plots show linear parts in the range of low substrate concentrations (B_∞) in the Figures 11S, 12S, 13S, 15S, 16S, 17S and none linear parts in the range of high substrate concentrations. Therefore they can yield correct values of Michaelis constants (K_B) and the maximum flux of the enzymatic reduction of NAD^+ (LV_1) in the range of low substrate concentrations even if the maximum response of the biosensors is limited by the rate of NADH oxidation at the electrode surface. That is true only if the transport of substrate is not a limiting factor. Certainly, the intercepts of none linear parts of Eadie-Hofstee plots with the axis of j give the correct values of the maximum response to glucose.

The Figures 19S-22S illustrate the influence of the maximum flux of the enzymatic reduction of NAD^+ (LV_1), the NAD^+ loading (A_t), and the mass transfer constant of the substrate (k'_B) on response of biosensors. The smaller are the NAD^+ loading and the maximum fluxes of the enzymatic reduction of NAD^+ in comparison with the maximum flux of the electrochemical NADH oxidation, the straighter are the Eadie-Hofstee plots. At lower concentrations of the substrate (B_∞) the slopes of the Eadie-Hofstee plots and hence the apparent Michaelis constants depend very much on k'_B. The effect of this factor on the apparent Michaelis constant is less pronounced at high values of B_∞.

GLOSSARY

j_{el}	flux of reactants (mol cm^{-2} s^{-1})
j	current density (A cm^{-2})

k_3, k_4, k_5, k_6, k_7	rate constants of the elemental enzymatic reactions in forward direction (M^{-1} s^{-1}, M^{-1} s^{-1}, s^{-1}, s^{-1}, s^{-1} , respectively)
k_{-3}, k_{-4}, k_{-5}, k_{-6}, k_{-7}	rate constants of the elemental enzymatic reactions in backward direction (s^{-1}, s^{-1}, s^{-1}, M^{-1} s^{-1}, and M^{-1} s^{-1}, respectively)
k'_B	mass transfer rate coefficient for the substrate (cm s^{-1})
k'_Q	mass transfer rate coefficient for the product (cm s^{-1})
L	thickness of a hydrogel layer (cm)
P_{im}	concentration of NADH immobilized in the hydrogel (M)
V_1	maximum velocity of the enzymatic reaction in forward direction (s^{-1})
V_2	maximum velocity of the enzymatic reaction in reverse direction (s^{-1})

Greek letters

Γ	total surface coverage of Os-phendione-PVP (mol cm^{-2})
Γ_{Mox}	surface coverage of the mediator in the oxidized form (mol cm^{-2})
Γ_{Mred}	surface coverage of the mediator in the reduced form (mol cm^{-2})
$\Gamma_{M \cdot P}$	surface coverage of the intermediate complex between Os-phendione-PVP and NADH (mol cm^{-2})

FIGURES AND FIGURE LEGENDS

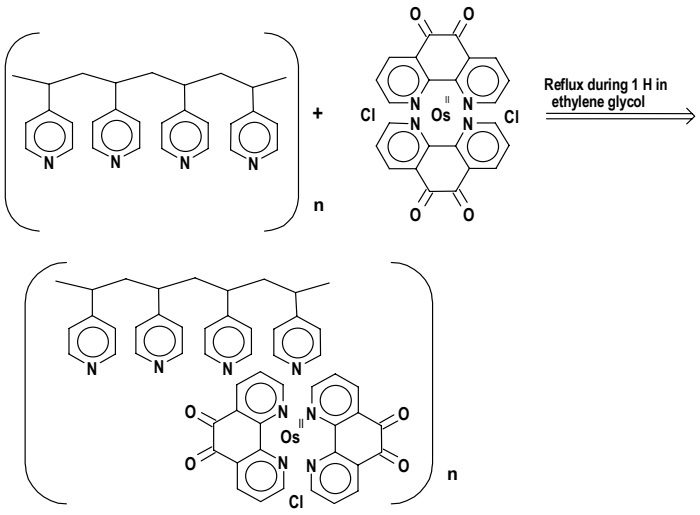

Figure 1S. The synthetic route to Os-phendione-PVP.

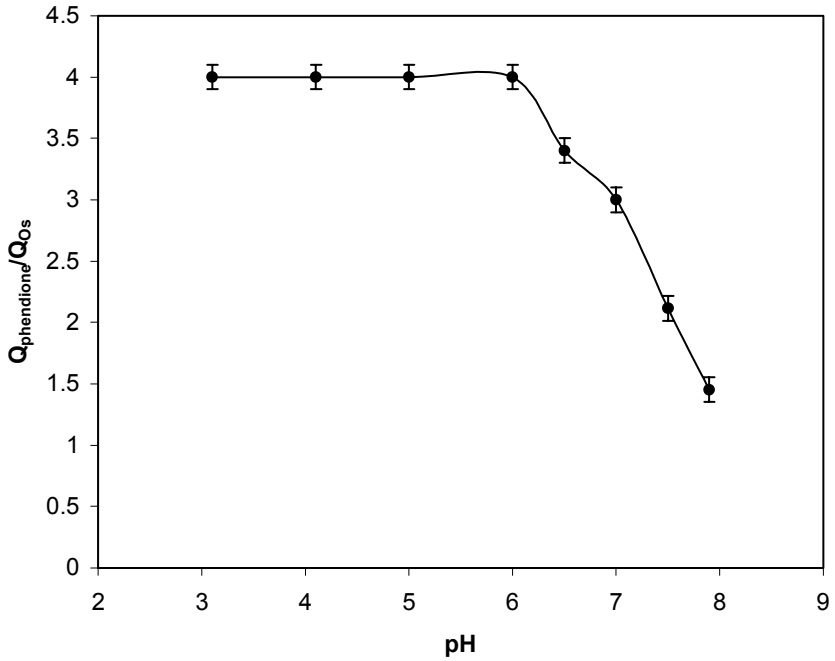

Figure 2S. The effect of pH on the ratio of phendione peak area to that of osmium atom in cyclic voltammetry.

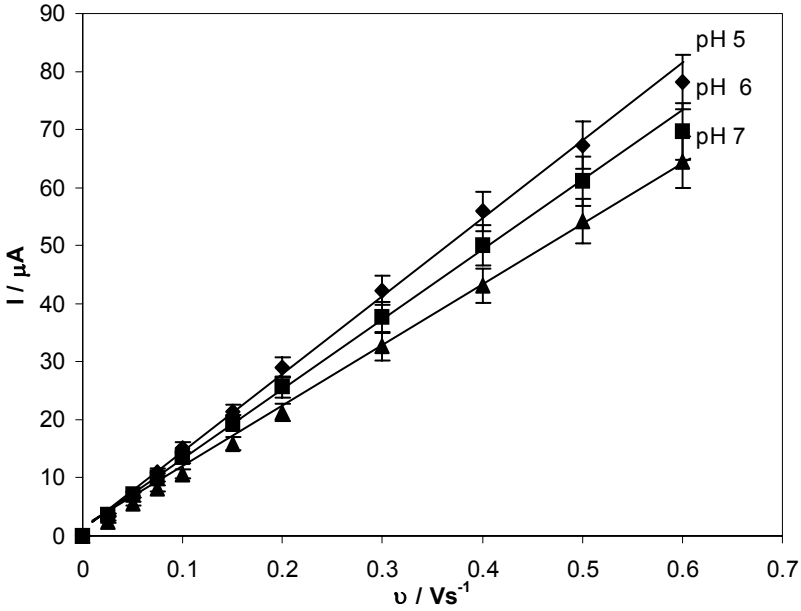

Figure 3S. The effect of scan rate on the anodic peak current of phendione. Experimental conditions: Os-phendione-PVP coverage (6.7± 0.5)x10^{-10} mol cm^{-2}, 0.1 M phosphate buffer.

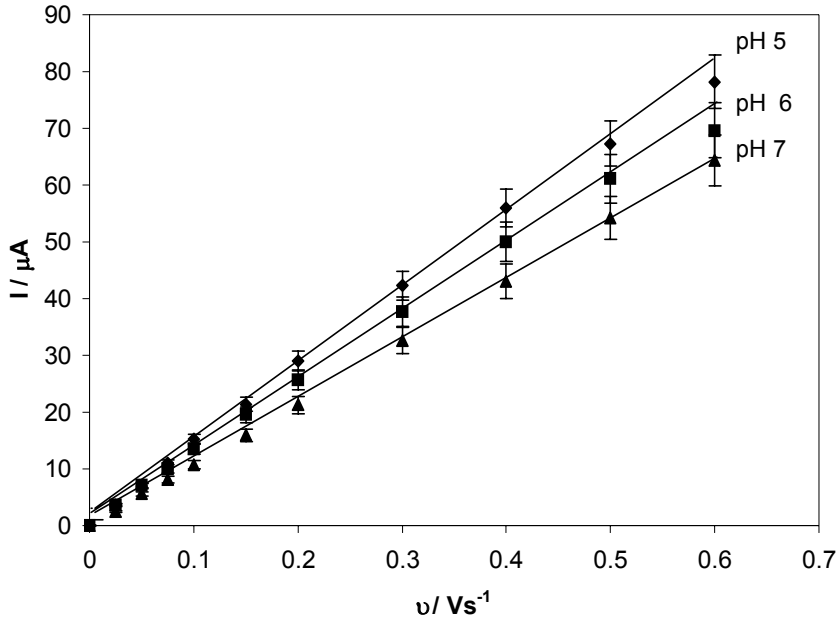

Figure 4S. The effect of scan rate on the cathodic peak current of phendione. Experimental conditions are the same as in Figure 3S.

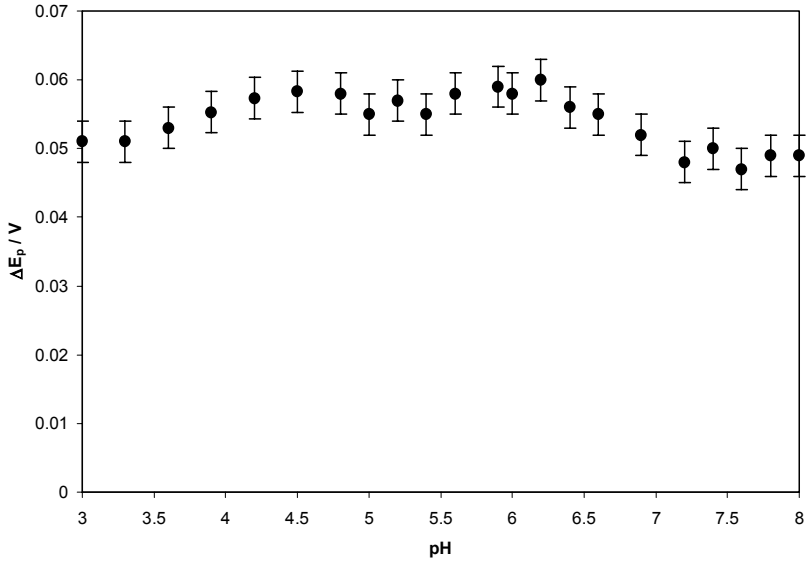

Figure 5S. Variation of ΔE_p as a function of pH. Experimental conditions are the same as in Figure 2.

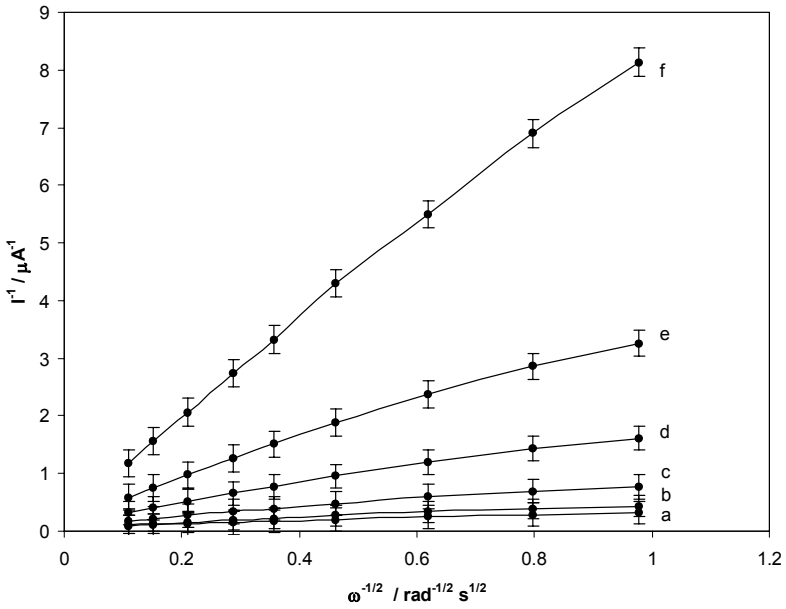

Figure 6S. Koutecky-Levich plot of steady state electrocatalytic response for an Os-phendione-PVP modified graphite RDE at different NADH concentrations: a) 0.05 mM; b) 0.1 mM; c) 0.2 mM; d) 0.4 mM; e) 0.8 mM; f) 1.2 mM. Experimental conditions: Os-phendione-PVP coverage $(7.3\pm0.3)\times10^{-10}$ mol cm^{-2}; applied potential 200 mV *vs.* Ag/AgCl/KCl_{sat}, 0.1 M phosphate buffer, pH 5.0, dearated with argon.

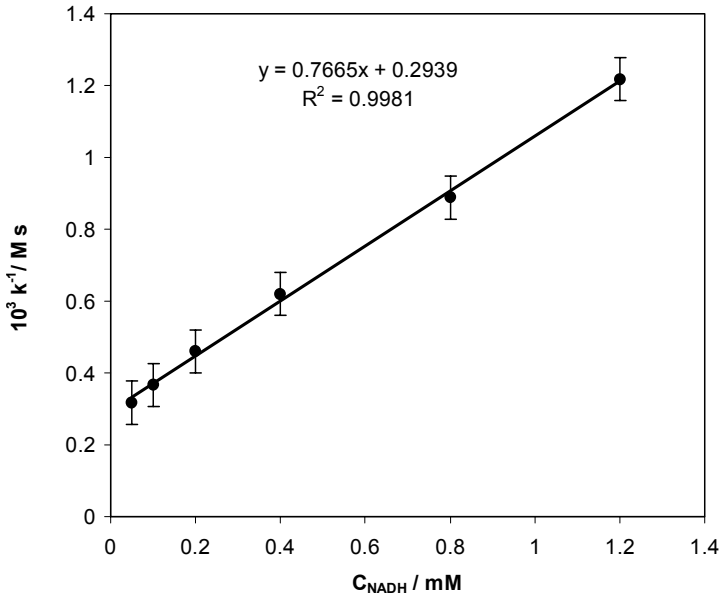

Figure 7S. Plot of k^{-1} *vs.* concentration of NADH for the electrooxidation of NADH at Os-phendione-PVP modified electrodes. Experimental conditions are the same as in Figure 6S.

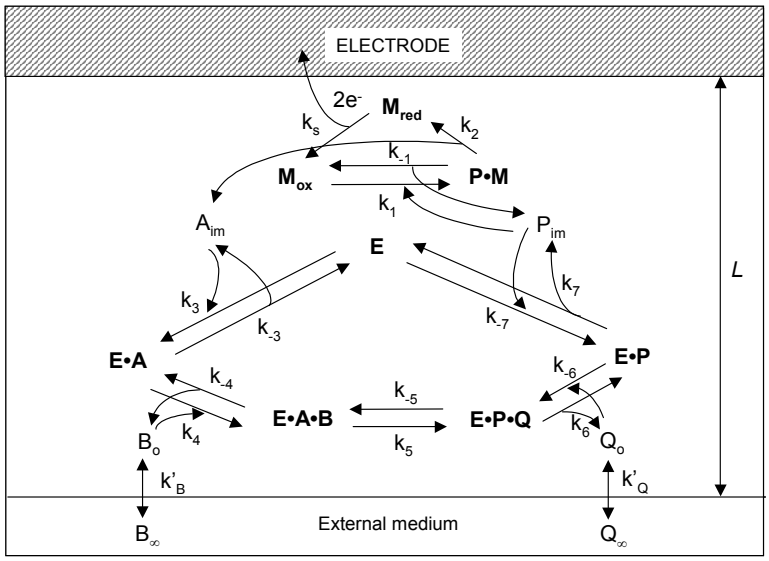

Figure 8S. Reaction scheme for a reagentless glucose biosensor.

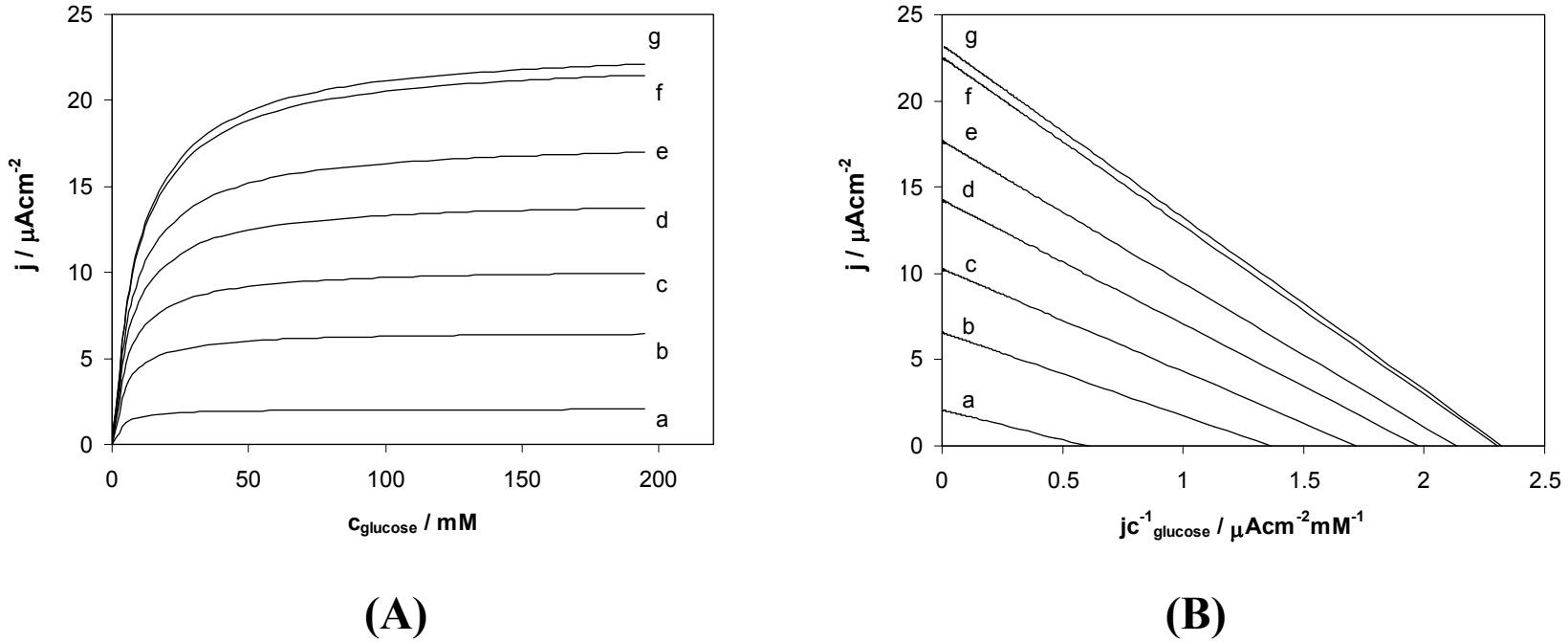

Figure 9S. Simulation of calibration curves **(A)** and Eadie-Hofstee plots **(B)** for the reagentless glucose biosensors with varying loading of NAD^+ in the hydrogel (A_t): a) 0.2 mM; b) 0.8 mM; c) 1.6 mM; d) 3.2 mM; e) 6.4 mM; f) 64 mM; g) ∞. The values of other parameters are: Γk_{cat} = 2.55x10^{-9} mol s^{-1} cm^{-2}; LV_l =1.2046x10^{-10} mol s^{-1} cm^{-2}; $k'_B \rightarrow \infty$; K_A=2 mM; K_B=10 mM; K_{AB} =5.6 mM^2; K_M=0.8 mM.

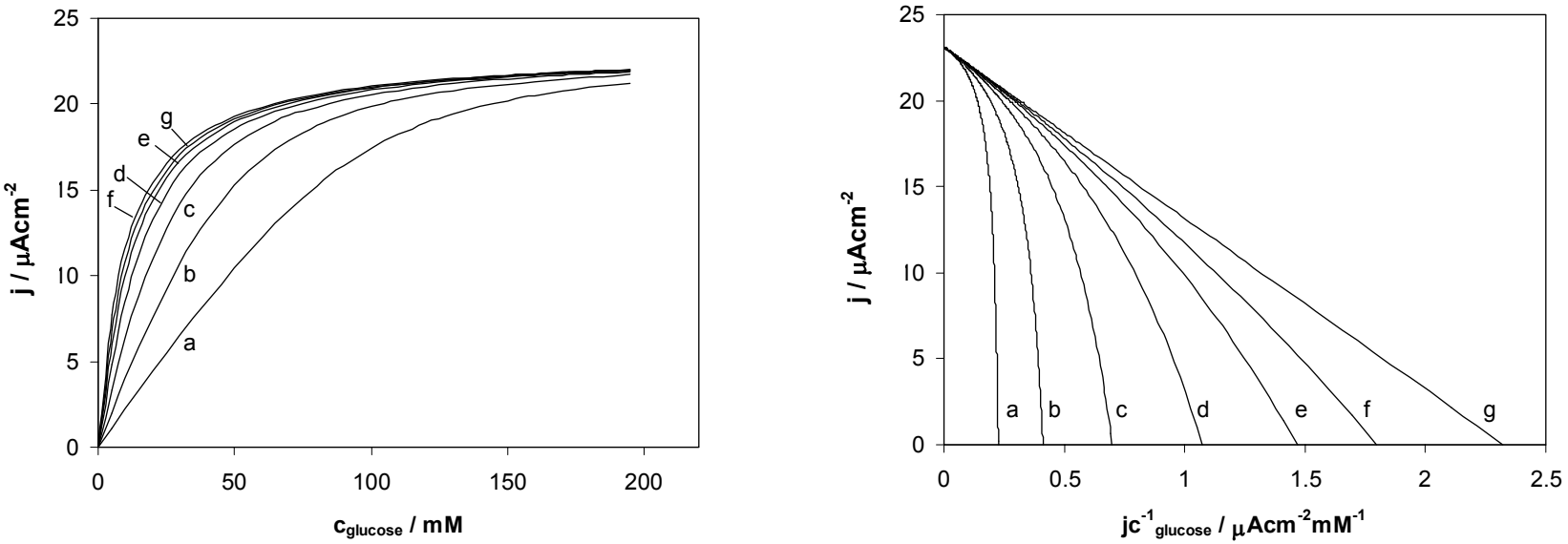

Figure 10S. Simulation of calibration curves **(A)** and Eadie-Hofstee plots **(B)** for the reagentless glucose biosensors with varying mass transfer coefficient (k'_B): a) 1.3×10^{-12} cm s^{-1}; b) 2.6×10^{-12} cm s^{-1}; c) 5.18×10^{-12} cm s^{-1}; d) 1.04×10^{-11} cm s^{-1}; e) 2.07×10^{-11} cm s^{-1}; f) 4.15×10^{-11} cm s^{-1}; g) ∞. The values of other parameters are: $A_t \rightarrow \infty$; $\Gamma k_{cat} = 2.55\times10^{-9}$ mol s^{-1} cm^{-2}; $LV_1 = 1.2046\times10^{-10}$ mol s^{-1} cm^{-2}; K_A=2 mM; K_B = 10 mM; K_{AB} = 5.6 mM^2; K_M = 0.8 mM.

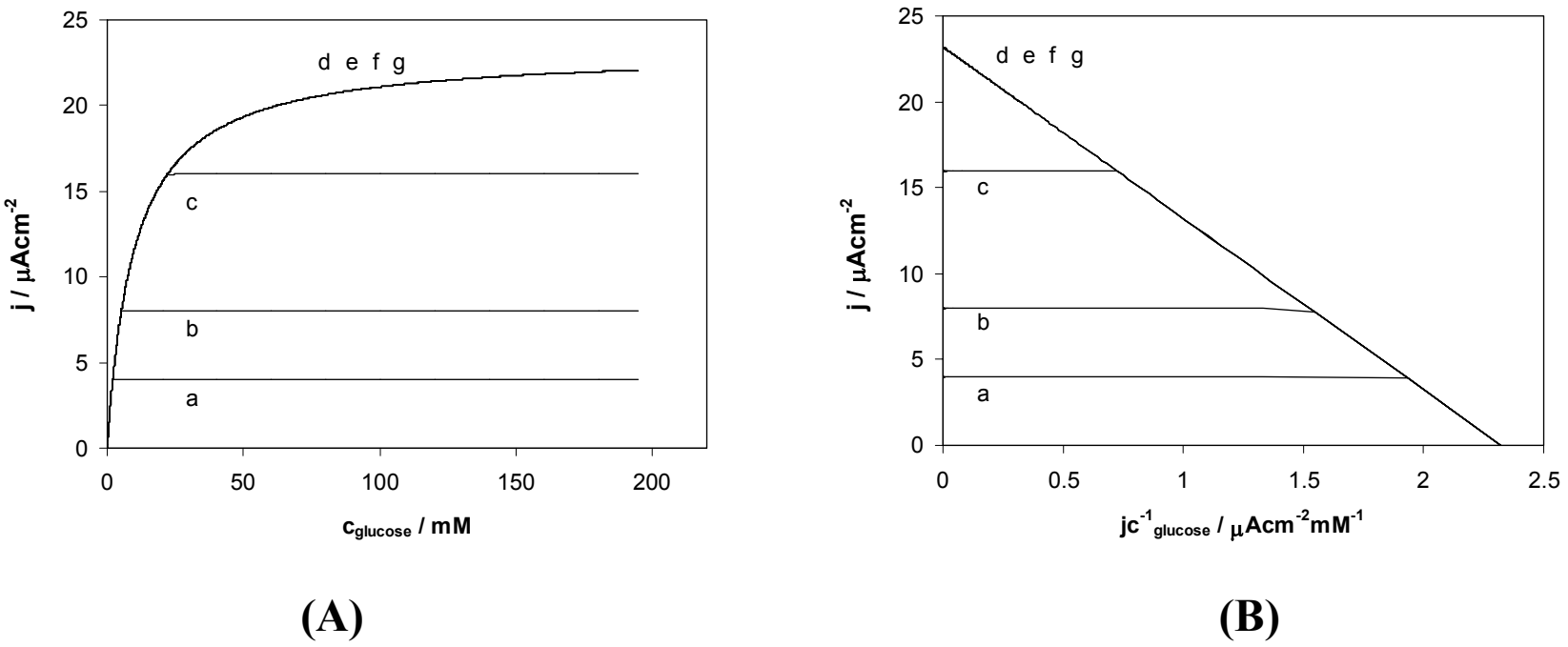

Figure 11S. Simulation of calibration curves **(A)** and Eadie-Hofstee plots **(B)** for the reagentless glucose biosensors at $A_t \rightarrow \infty$ with varying maximum fluxes of the electrochemical NADH oxidation (Γk_{cat}): a) 2.073x10^{-11} mol s^{-1} cm^{-2}; b) 4.145x10^{-11} mol s^{-1} cm^{-2}; c) 8.291x10^{-11} mol s^{-1} cm^{-2}; d) 1.204x10^{-10} mol s^{-1} cm^{-2}; e) 2.073x10^{-10} mol s^{-1} cm^{-2}; f) 4.145x10^{-10} mol s^{-1} cm^{-2}; g) ∞. The values of other parameters are: $k'_B \rightarrow \infty$; LV_1 = 1.204x10^{-10} mol s^{-1} cm^{-2}; K_A=2 mM; K_B = 10 mM; K_{AB} = 5.6 mM^2; K_M = 0.8 mM.

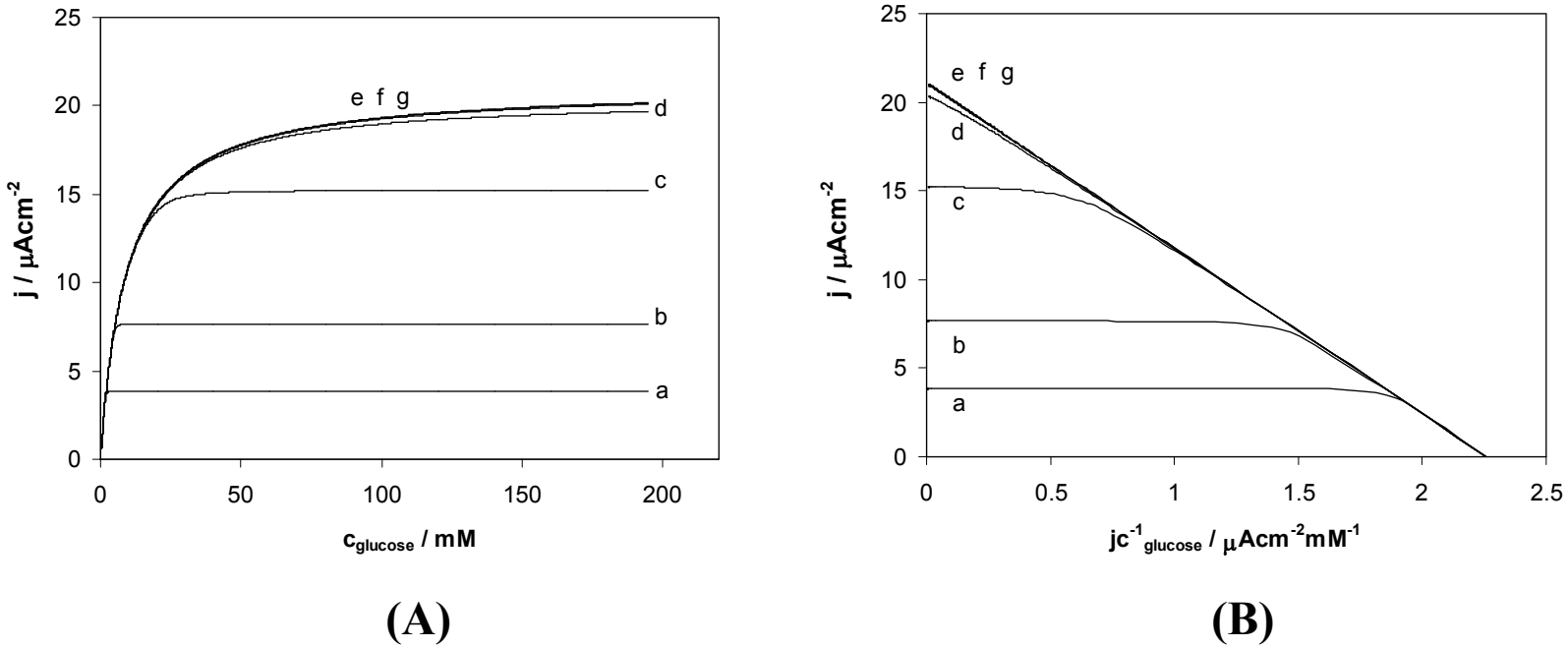

Figure 12S. Simulation of calibration curves **(A)** and Eadie-Hofstee plots **(B)** for the reagentless glucose biosensors at A_t equal to 20 mM with varying maximum fluxes of the electrochemical NADH oxidation (Γk_{cat}): a) 2.073×10^{-11} mol s^{-1} cm^{-2}; b) 4.145×10^{-11} mol s^{-1} cm^{-2}; c) 8.291×10^{-11} mol s^{-1} cm^{-2}; d) 1.204×10^{-10} mol s^{-1} cm^{-2}; e) 2.073×10^{-10} mol s^{-1} cm^{-2}; f) 4.145×10^{-10} mol s^{-1} cm^{-2}; g) ∞. The values of other parameters are: $k'_B \rightarrow \infty$; $LV_1 = 1.204 \times 10^{-10}$ mol s^{-1} cm^{-2}; K_A=2 mM; K_B = 10 mM; K_{AB} = 5.6 mM^2; K_M = 0.8 mM.

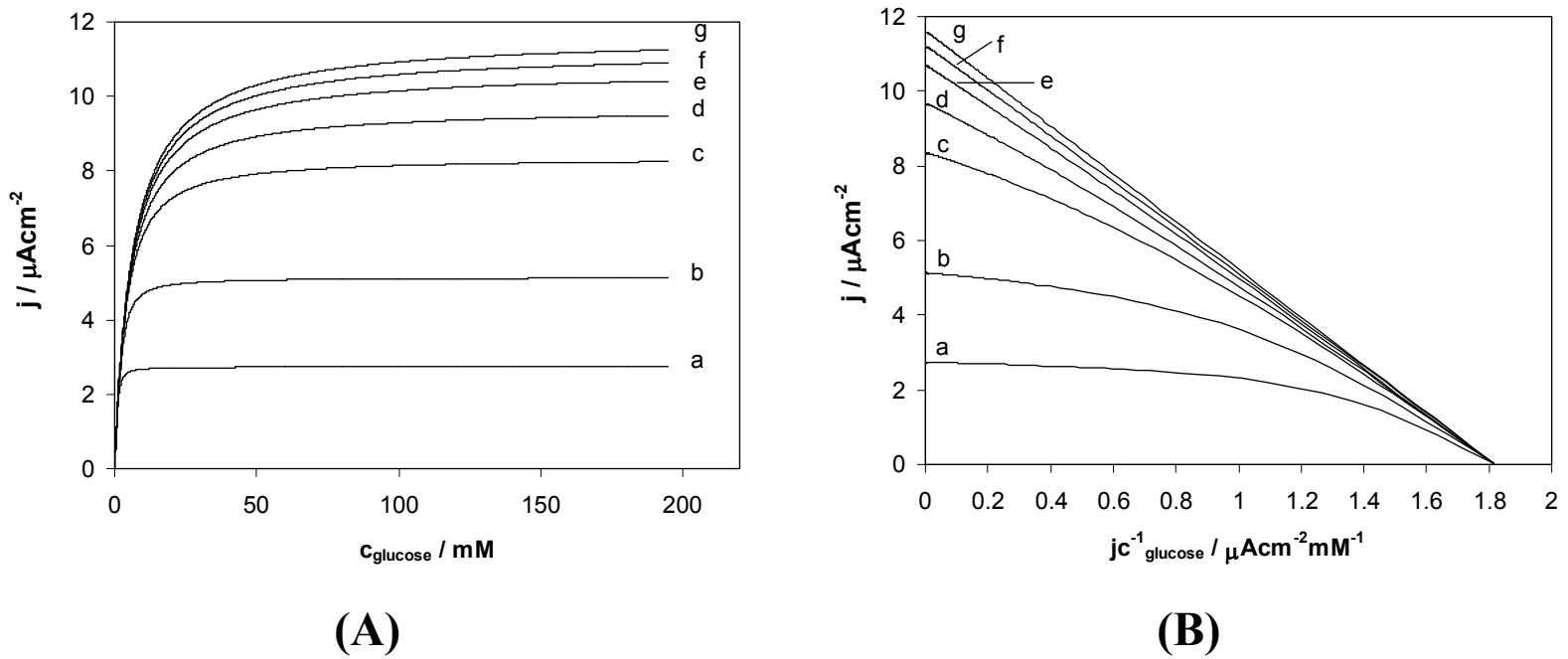

Figure 13S. Simulation of calibration curves **(A)** and Eadie-Hofstee plots **(B)** for the reagentless glucose biosensors at A_t equal to 2 mM with varying maximum fluxes of the electrochemical NADH oxidation (Γk_{cat}): a) 2.073×10^{-11} mol s^{-1} cm^{-2}; b) 4.145×10^{-11} mol s^{-1} cm^{-2}; c) 8.291×10^{-11} mol s^{-1} cm^{-2}; d) 1.204×10^{-10} mol s^{-1} cm^{-2}; e) 2.073×10^{-10} mol s^{-1} cm^{-2}; f) 4.145×10^{-10} mol s^{-1} cm^{-2}; g) ∞. The values of other parameters are: $k'_B \rightarrow \infty$; $LV_1 = 1.204 \times 10^{-10}$ mol s^{-1} cm^{-2}; K_A=2 mM; K_B = 10 mM; K_{AB} = 5.6 mM^2; K_M = 0.8 mM.

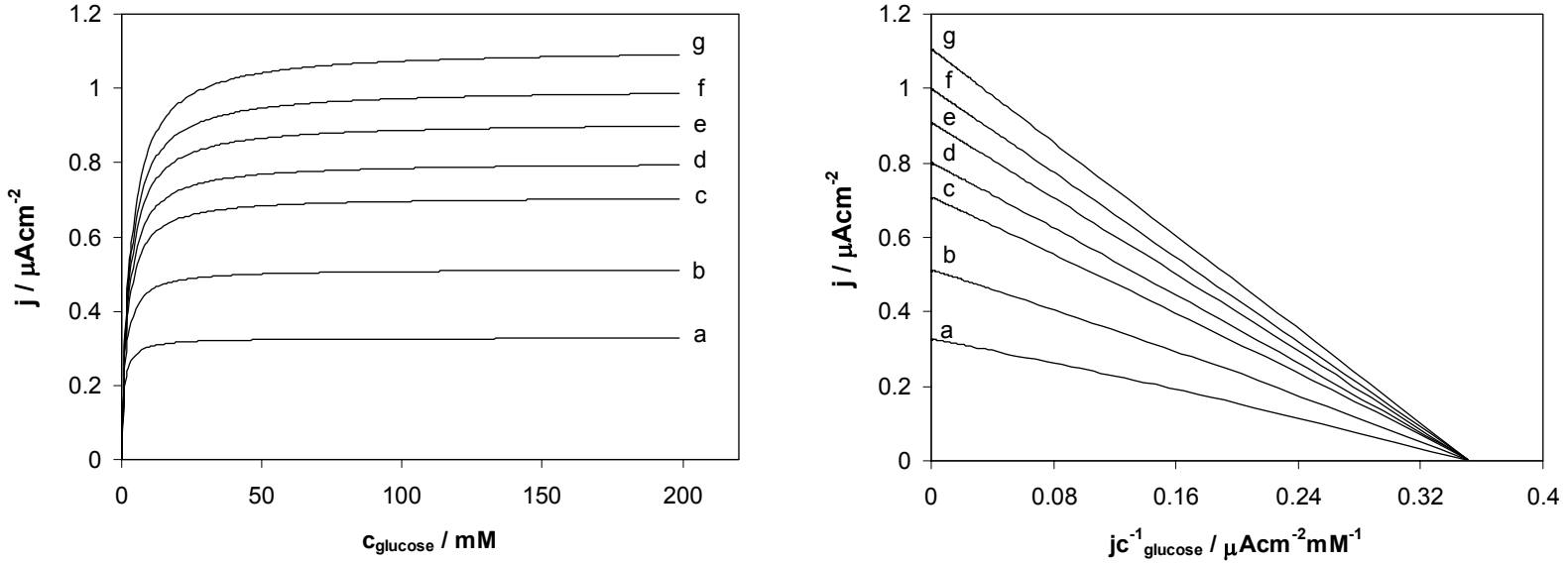

Figure 14S. Simulation of calibration curves **(A)** and Eadie-Hofstee plots **(B)** for the reagentless glucose biosensors at A_t equal to 0.1 mM with varying maximum fluxes of the electrochemical NADH oxidation (Γk_{cat}): a) 2.073x10^{-11} mol s^{-1} cm^{-2}; b) 4.145x10^{-11} mol s^{-1} cm^{-2}; c) 8.291x10^{-11} mol s^{-1} cm^{-2}; d) 1.204x10^{-10} mol s^{-1} cm^{-2}; e) 2.073x10^{-10} mol s^{-1} cm^{-2}; f) 4.145x10^{-10} mol s^{-1} cm^{-2}; g) ∞. The values of other parameters are: $k'_B \rightarrow \infty$; LV_1 = 1.204x10^{-10} mol s^{-1} cm^{-2}; K_A=2 mM; K_B = 10 mM; K_{AB} = 5.6 mM^2; K_M = 0.8 mM.

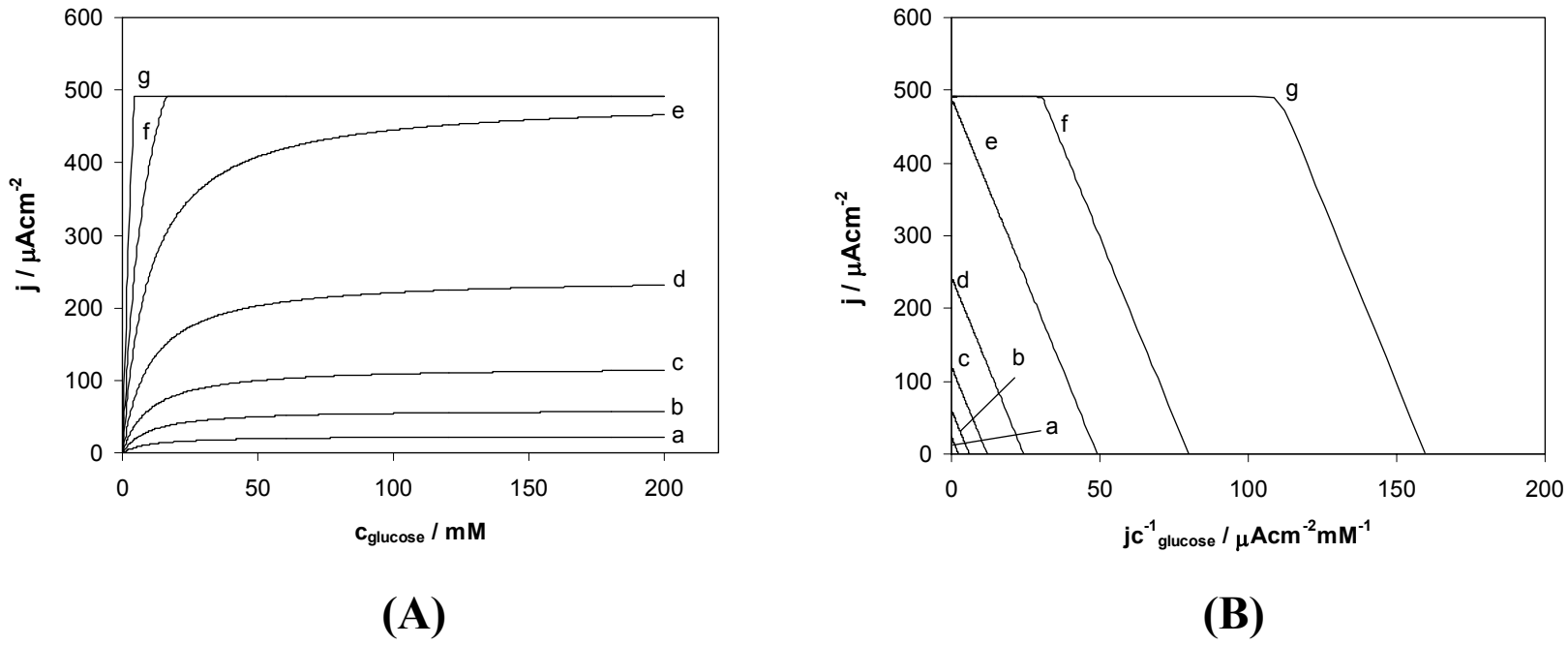

Figure 15S. Simulation of calibration curves **(A)** and Eadie-Hofstee plots **(B)** for the reagentless glucose biosensors at $A_t \rightarrow \infty$ with varying maximum fluxes of the enzymatic reduction of NAD^+ (LV_1): a) 1.204×10^{-10} mol s^{-1} cm^{-2}; b) 3.109×10^{-10} mol s^{-1} cm^{-2}; c) 6.218×10^{-10} mol s^{-1} cm^{-2}; d) 1.264×10^{-9} mol s^{-1} cm^{-2}; e) 2.549×10^{-9} mol s^{-1} cm^{-2}; f) 4.146×10^{-9} mol s^{-1} cm^{-2}; g) 8.281×10^{-9} mol s^{-1} cm^{-2}. The values of other parameters are: $k'_B \rightarrow \infty$; Γk_{cat} = 2.549×10^{-9} mol s^{-1} cm^{-2}; K_A=2 mM; K_B = 10 mM; K_{AB} = 5.6 mM^2; K_M = 0.8 mM

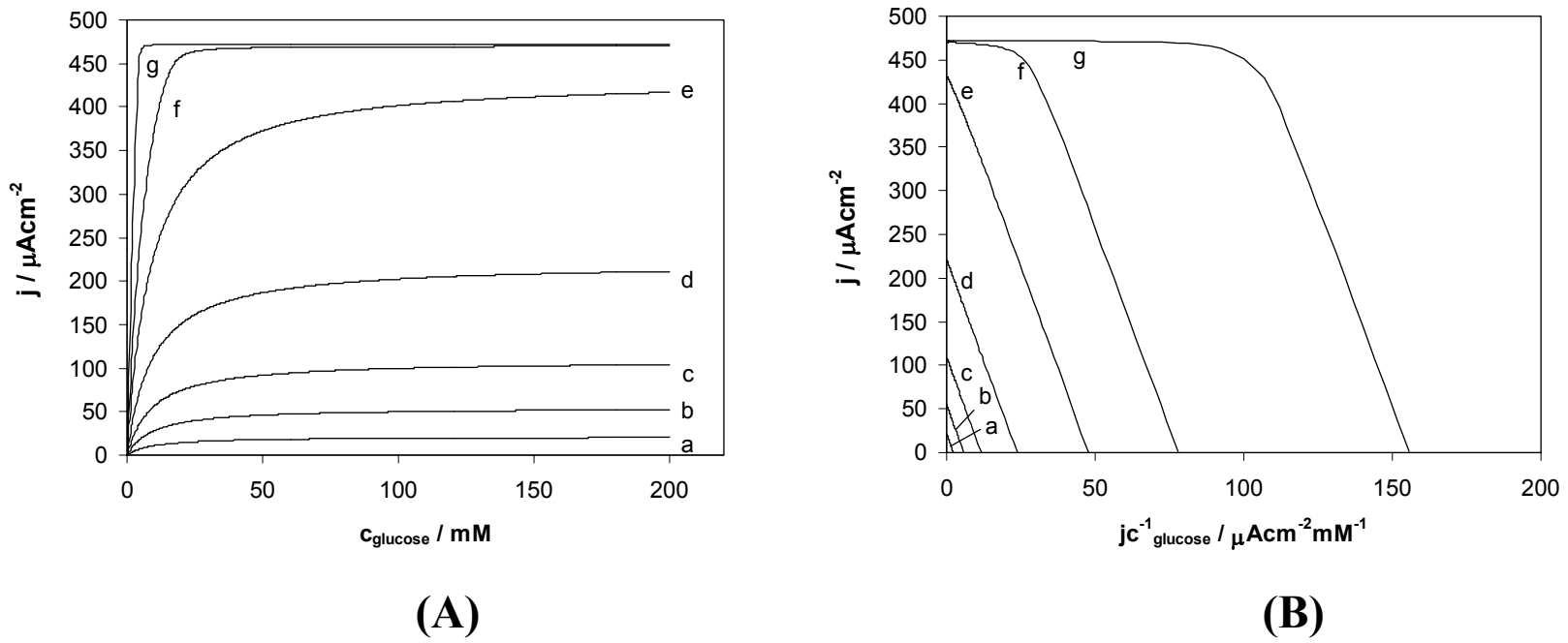

Figure 16S. Simulation of calibration curves **(A)** and Eadie-Hofstee plots **(B)** for the reagentless glucose biosensors at A_t equal to 20 mM with varying maximum fluxes of the enzymatic reduction of NAD^+ (LV_1): a) 1.204×10^{-10} mol s^{-1} cm^{-2}; b) 3.109×10^{-10} mol s^{-1} cm^{-2}; c) 6.218×10^{-10} mol s^{-1} cm^{-2}; d) 1.264×10^{-9} mol s^{-1} cm^{-2}; e) 2.549×10^{-9} mol s^{-1} cm^{-2}; f) 4.146×10^{-9} mol s^{-1} cm^{-2}; g) 8.281×10^{-9} mol s^{-1} cm^{-2}. The values of other parameters are: $k'_B \rightarrow \infty$; Γk_{cat} = 2.549×10^{-9} mol s^{-1} cm^{-2}; K_A=2 mM; K_B = 10 mM; K_{AB} = 5.6 mM^2; K_M = 0.8 mM.

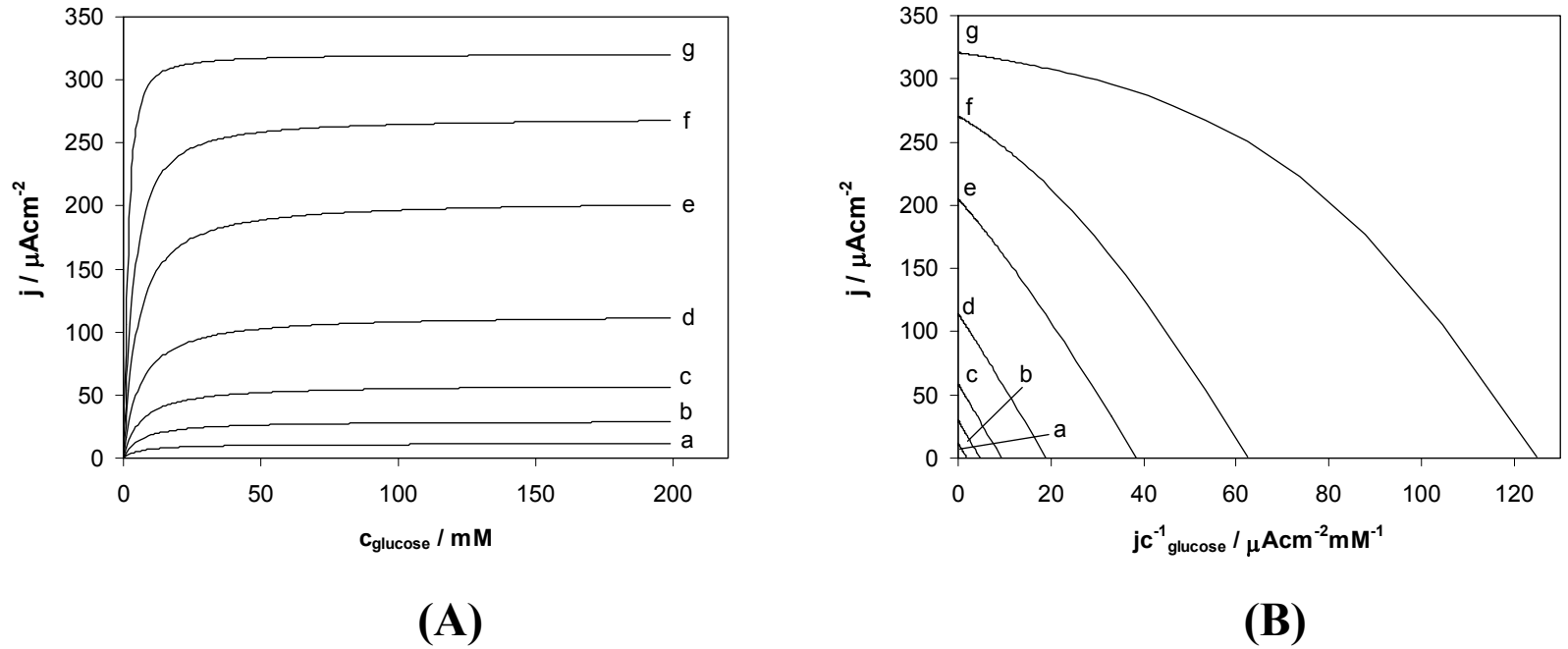

Figure 17S. Simulation of calibration curves **(A)** and Eadie-Hofstee plots **(B)** for the reagentless glucose biosensors at A_t equal to 2.0 mM with varying maximum fluxes of the enzymatic reduction of NAD^+ (LV_1): a) 1.204×10^{-10} mol s^{-1} cm^{-2}; b) 3.109×10^{-10} mol s^{-1} cm^{-2}; c) 6.218×10^{-10} mol s^{-1} cm^{-2}; d) 1.264×10^{-9} mol s^{-1} cm^{-2}; e) 2.549×10^{-9} mol s^{-1} cm^{-2}; f) 4.146×10^{-9} mol s^{-1} cm^{-2}; g) 8.281×10^{-9} mol s^{-1} cm^{-2}. The values of other parameters are: $k'_B \rightarrow \infty$; $\Gamma k_{cat} = 2.549 \times 10^{-9}$ mol s^{-1} cm^{-2}; K_A=2 mM; K_B = 10 mM; K_{AB} = 5.6 mM^2; K_M = 0.8 mM

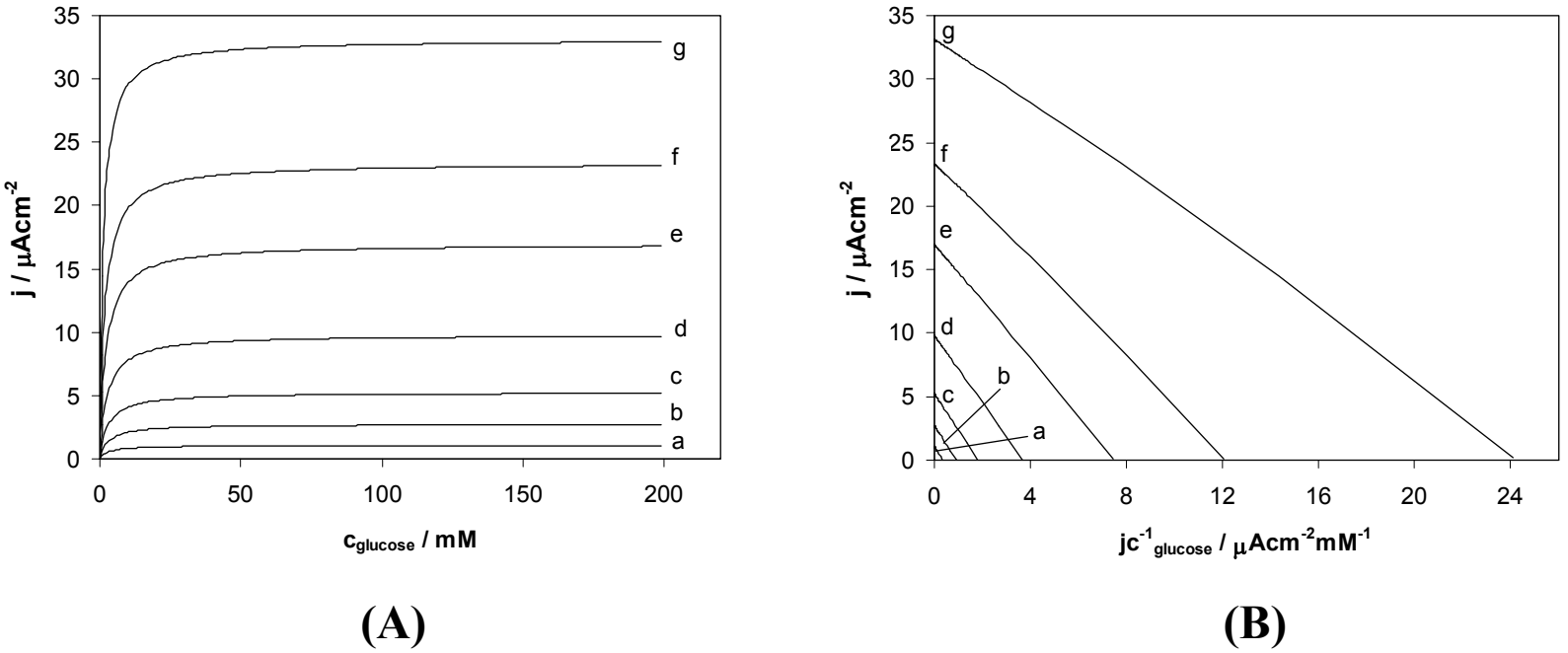

Figure 18S. Simulation of calibration curves **(A)** and Eadie-Hofstee plots **(B)** for the reagentless glucose biosensors at A_t equal to 0.1 mM with varying maximum fluxes of the enzymatic reduction of NAD^+ (LV_1): a) 1.204×10^{-10} mol s^{-1} cm^{-2}; b) 3.109×10^{-10} mol s^{-1} cm^{-2}; c) 6.218×10^{-10} mol s^{-1} cm^{-2}; d) 1.264×10^{-9} mol s^{-1} cm^{-2}; e) 2.549×10^{-9} mol s^{-1} cm^{-2}; f) 4.146×10^{-9} mol s^{-1} cm^{-2}; g) 8.281×10^{-9} mol s^{-1} cm^{-2}. The values of other parameters are: $k'_B \rightarrow \infty$; Γk_{cat} = 2.549×10^{-9} mol s^{-1} cm^{-2}; K_A=2 mM; K_B = 10 mM; K_{AB} = 5.6 mM^2; K_M = 0.8 mM.

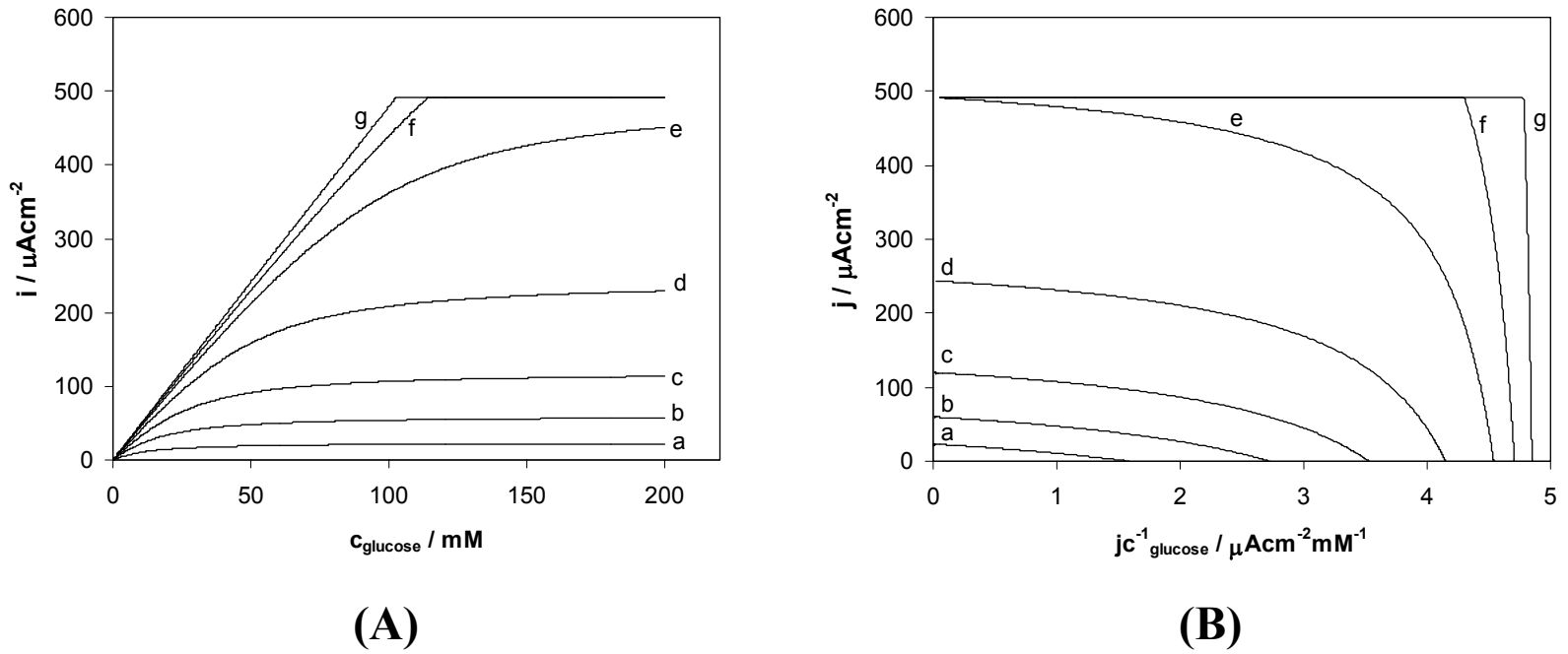

Figure 19S. Simulation of calibration curves **(A)** and Eadie-Hofstee plots **(B)** for the reagentless glucose biosensors at k'_B equal to 2.591×10^{-11} cm s^{-1} and $A_t \rightarrow \infty$ with varying maximum fluxes of the enzymatic reduction of NAD^+ (LV_1): a) 1.204×10^{-10} mol s^{-1} cm^{-2}; b) 3.109×10^{-10} mol s^{-1} cm^{-2}; c) 6.218×10^{-10} mol s^{-1} cm^{-2}; d) 1.264×10^{-9} mol s^{-1} cm^{-2}; e) 2.549×10^{-9} mol s^{-1} cm^{-2}; f) 4.146×10^{-9} mol s^{-1} cm^{-2}; g) 8.281×10^{-9} mol s^{-1} cm^{-2}. The values of other parameters are: $\Gamma k_{cat} = 2.549 \times 10^{-9}$ mol s^{-1} cm^{-2}; K_A=2 mM; K_B = 10 mM; K_{AB} = 5.6 mM^2; K_M = 0.8 mM.

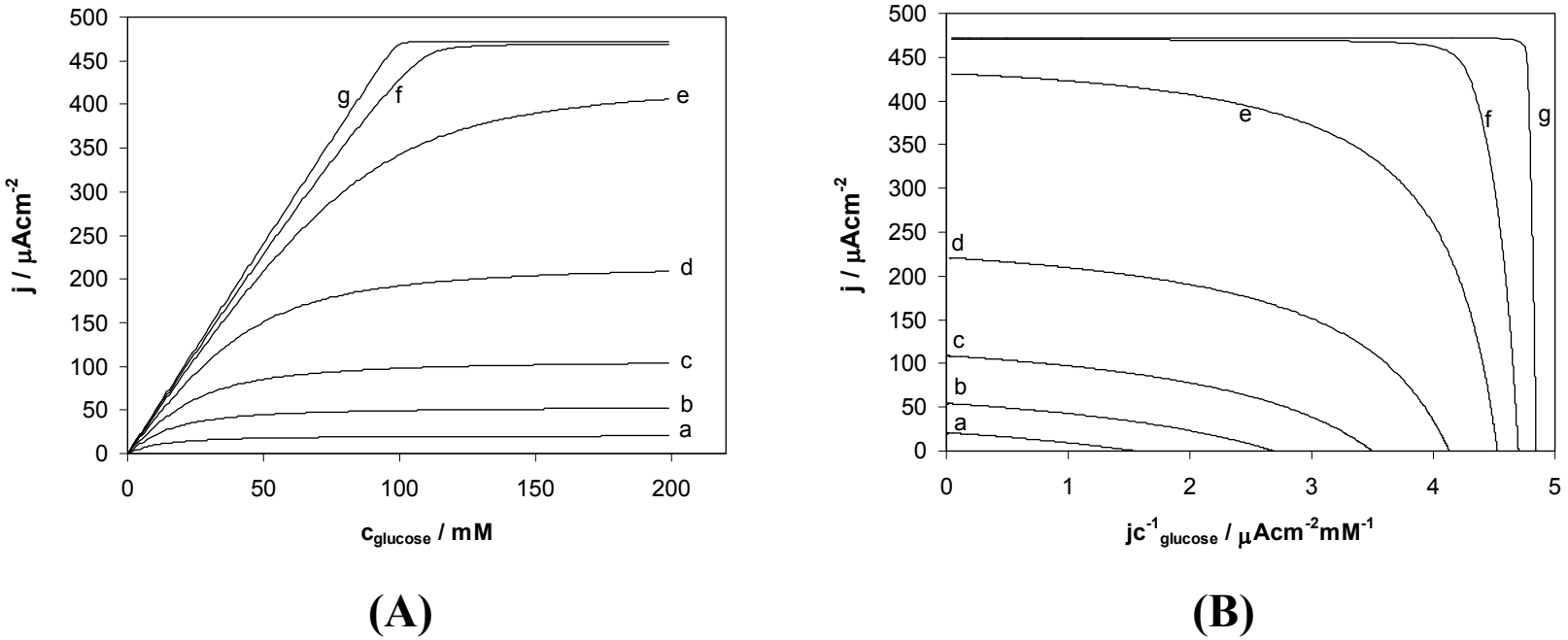

Figure 20S. Simulation of calibration curves **(A)** and Eadie-Hofstee plots **(B)** for the reagentless glucose biosensors at k'_B equal to 2.591×10^{-11} cm s^{-1} and A_t equal to 20 mM with varying maximum fluxes of the enzymatic reduction of NAD^+ (LV_1): a) 1.204×10^{-10} mol s^{-1} cm^{-2}; b) 3.109×10^{-10} mol s^{-1} cm^{-2}; c) 6.218×10^{-10} mol s^{-1} cm^{-2}; d) 1.264×10^{-9} mol s^{-1} cm^{-2}; e) 2.549×10^{-9} mol s^{-1} cm^{-2}; f) 4.146×10^{-9} mol s^{-1} cm^{-2}; g) 8.281×10^{-9} mol s^{-1} cm^{-2}. The values of other parameters are: Γk_{cat} = 2.549×10^{-9} mol s^{-1} cm^{-2}; K_A=2 mM; K_B = 10 mM; K_{AB} = 5.6 mM^2; K_M = 0.8 mM.

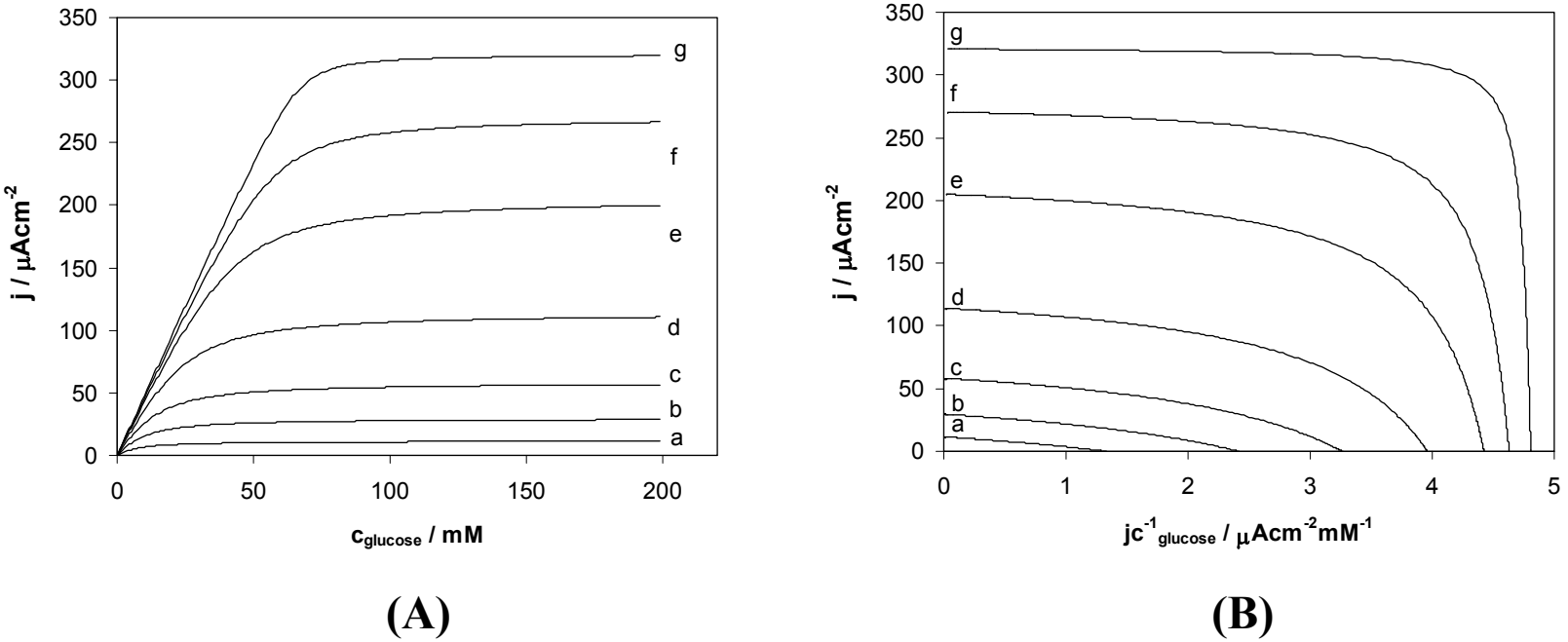

Figure 21S. Simulation of calibration curves **(A)** and Eadie-Hofstee plots **(B)** for the reagentless glucose biosensors at k'_B equal to 2.591×10^{-11} cm s^{-1} and A_t equal to 2.0 mM with varying maximum fluxes of the enzymatic reduction of NAD^+ (LV_1): a) 1.204×10^{-10} mol s^{-1} cm^{-2}; b) 3.109×10^{-10} mol s^{-1} cm^{-2}; c) 6.218×10^{-10} mol s^{-1} cm^{-2}; d) 1.264×10^{-9} mol s^{-1} cm^{-2}; e) 2.549×10^{-9} mol s^{-1} cm^{-2}; f) 4.146×10^{-9} mol s^{-1} cm^{-2}; g) 8.281×10^{-9} mol s^{-1} cm^{-2}. The values of other parameters are: Γk_{cat} = 2.549×10^{-9} mol s^{-1} cm^{-2}; K_A=2 mM; K_B = 10 mM; K_{AB} = 5.6 mM^2; K_M = 0.8 mM.

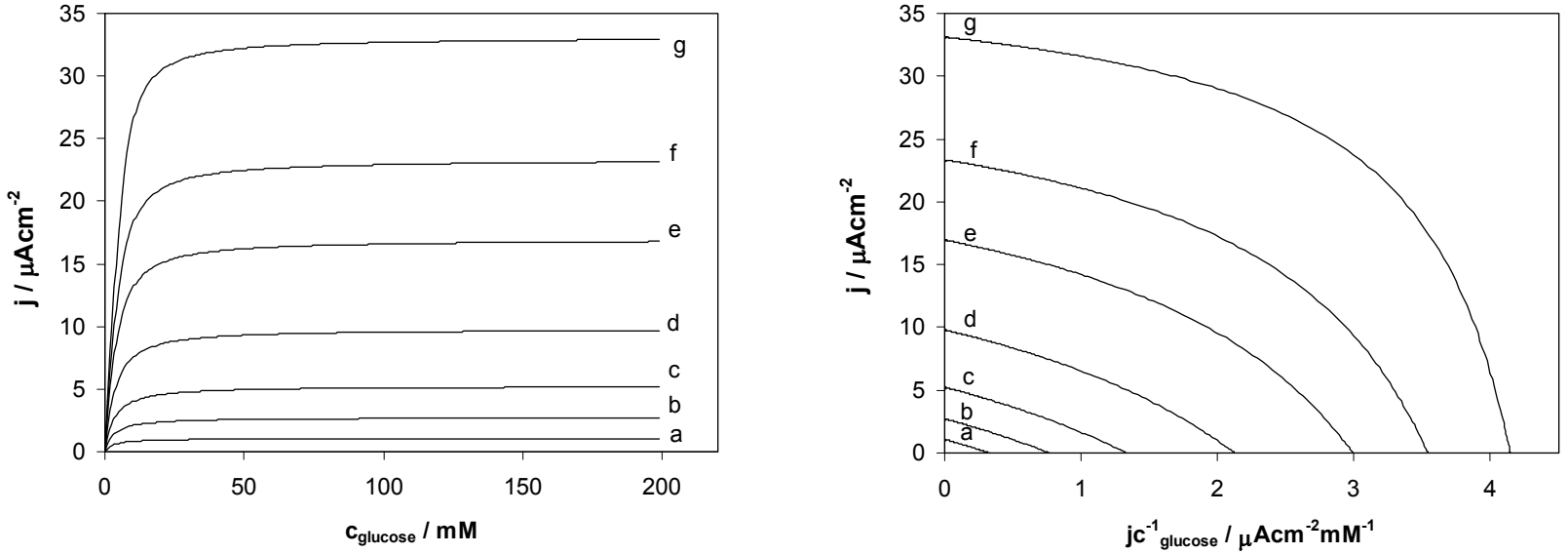

(A) **(B)**

Figure 22S. Simulation of calibration curves **(A)** and Eadie-Hofstee plots **(B)** for the reagentless glucose biosensors at k'_B equal to 2.591×10^{-11} cm s^{-1} and A_t equal to 0.1 mM with varying maximum fluxes of the enzymatic reduction of NAD^+ (LV_1): a) 1.204×10^{-10} mol s^{-1} cm^{-2}; b) 3.109×10^{-10} mol s^{-1} cm^{-2}; c) 6.218×10^{-10} mol s^{-1} cm^{-2}; d) 1.264×10^{-9} mol s^{-1} cm^{-2}; e) 2.549×10^{-9} mol s^{-1} cm^{-2}; f) 4.146×10^{-9} mol s^{-1} cm^{-2}; g) 8.281×10^{-9} mol s^{-1} cm^{-2}. The values of other parameters are: Γk_{cat} = 2.549×10^{-9} mol s^{-1} cm^{-2}; K_A=2 mM; K_B = 10 mM; K_{AB} = 5.6 mM^2; K_M = 0.8 mM.

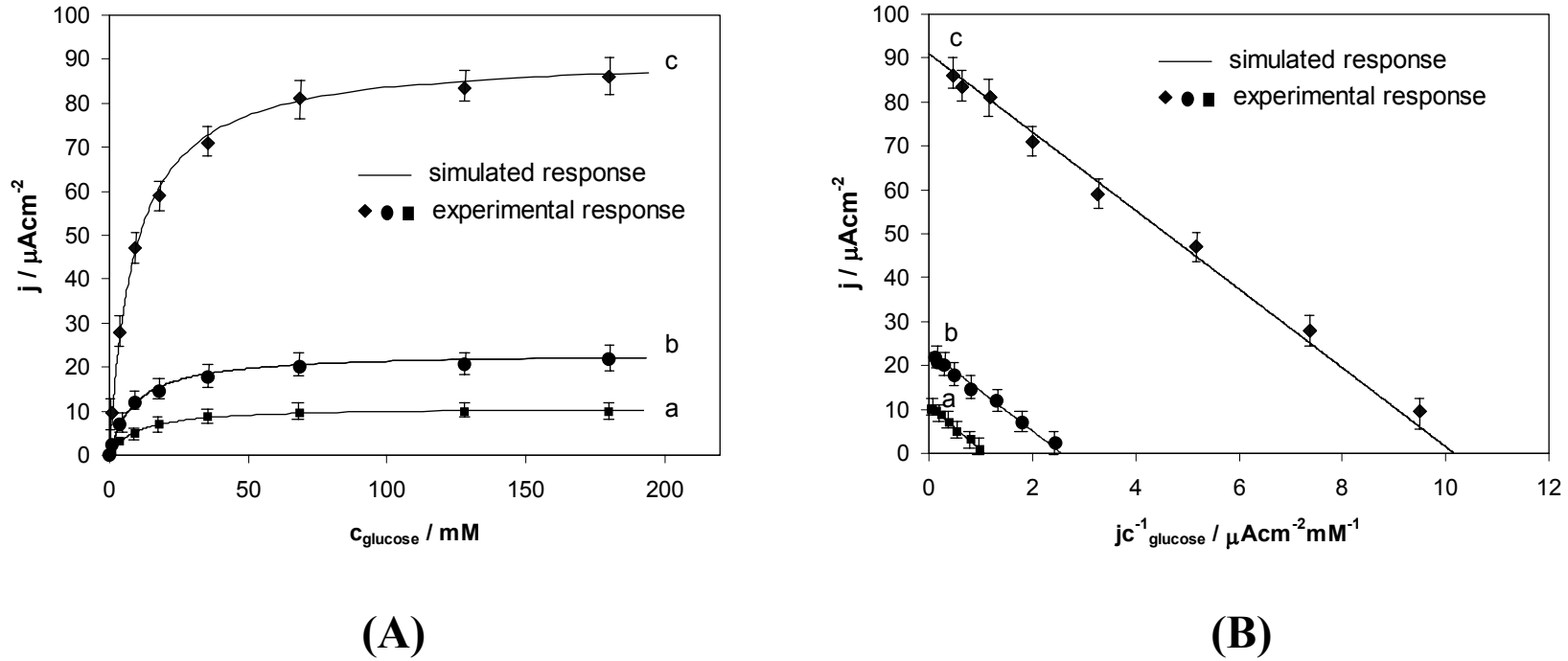

Figure 23S. Simulated and experimental calibration curves **(A)** and Eadie-Hofstee plots **(B)** for the biosensors prepared using varied loading of GDH per electrode: a) 0.135 U; b) 0.027 U; c) 0.0135 U. Experimental conditions: temperature 25°C, applied potential 150 mV *vs.* Ag/AgCl/KCl_{sat}, 0.1 M phosphate buffer, pH 7.0, containing 26 mM NAD^+. The value of Γk_{cat} employed for fitting and simulation was 2.549×10^{-9} mol s^{-1} cm^{-2}. The values of K_B, LV_1, and k'_B found by fitting and employed for simulation are listed in Table III.

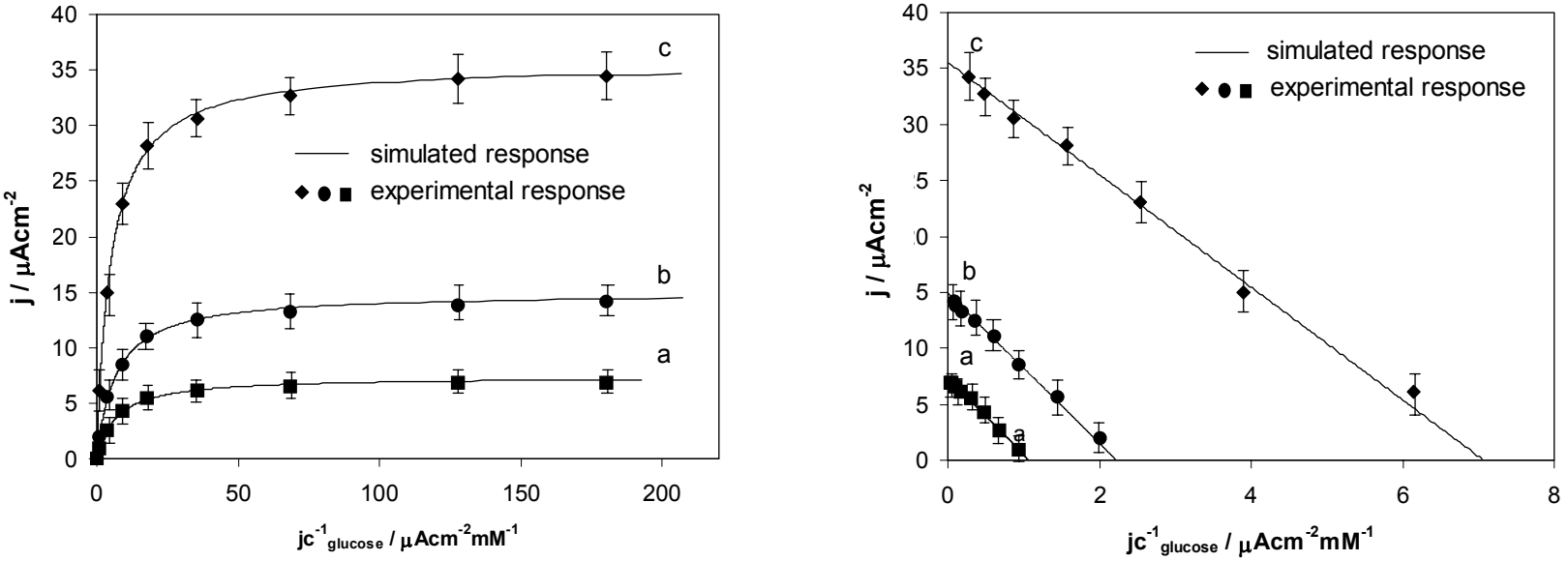

Figure 24S. Simulated and experimental calibration curves **(A)** and Eadie-Hofstee plots **(B)** for the biosensors operating in the reagentless mode prepared using varied loading of GDH per electrode: a) 0.135 U; b) 0.027; c) 0.0135 U. Experimental conditions: temperature 25°C, applied potential 150 mV *vs.* Ag/AgCl/KCl_{sat}, 0.1 M phosphate buffer, pH 7.0. The values of Γk_{cat} and K_M employed for fitting and simulation were 2.549×10^{-9} mol s^{-1} cm^{-2} and 0.8 mM respectively. The values of k'_B, K_A, K_{AB}, K_B, LV_1, and A_t found by fitting and employed for simulation are listed in Tables III and IV.